ALEX(01)-TR-75-08

APPLICATION OF P-WAVE SPECTRAL MEASUREMENTS TO SHORT-PERIOD DISCRIMINATION

TECHNICAL REPORT NO. 8

VELA NETWORK EVALUATION AND AUTOMATIC PROCESSING RESEARCH

Prepared by
Robert L. Sax

TEXAS INSTRUMENTS INCORPORATED
Equipment Group
Post Office Box 6015
Dallas, Texas 75222

Prepared for

AIR FORCE TECHNICAL APPLICATIONS CENTER
AFTAC Project No. VELA T/5705/B/ETR
Alexandria, Virginia 22314

Sponsored by

ADVANCED RESEARCH PROJECTS AGENCY
Nuclear Monitoring Research Office
ARPA Program Code No. 5F10
ARPA Order No. 2551

31 July 1975

Acknowledgment: This research was supported by the Advanced Research Projects Agency, Nuclear Monitoring Research Office, under Project VELA-UNIFORM, and accomplished under the technical direction of the Air Force Technical Applications Center under Contract Number F08606-75-C-0029.

ALEX(01)-TR-75-08

APPLICATION OF P-WAVE SPECTRAL MEASUREMENTS TO SHORT-PERIOD DISCRIMINATION

TECHNICAL REPORT NO. 8
VELA NETWORK EVALUATION AND AUTOMATIC PROCESSING RESEARCH

Prepared by
Robert L. Sax

TEXAS INSTRUMENTS INCORPORATED
Equipment Group
Post Office Box 6015
Dallas, Texas 75222

Prepared for
AIR FORCE TECHNICAL APPLICATIONS CENTER
AFTAC Project No. VELA T/5705/B/ETR
Alexandria, Virginia 22314

Sponsored by
ADVANCED RESEARCH PROJECTS AGENCY
Nuclear Monitoring Research Office
ARPA Program Code No. 5F10
ARPA Order No. 2551

31 July 1975

Acknowledgment: This research was supported by the Advanced Research Projects Agency, Nuclear Monitoring Research Office, under Project VELA-UNIFORM, and accomplished under the technical direction of the Air Force Technical Applications Center under Contract Number F08606-75-C-0029.

UNCLASSIFIED

SECURITY CLASSIFICATION OF THIS PAGE (When Data Entered)

REPORT DOCUMENTATION PAGE

READ INSTRUCTIONS BEFORE COMPLETING FORM

1. REPORT NUMBER
2. GOVT ACCESSION NO.
3. RECIPIENT'S CATALOG NUMBER

4. TITLE (and Subtitle)

APPLICATION OF P-WAVE SPECTRAL MEASUREMENTS TO SHORT-PERIOD DISCRIMINATION

5. TYPE OF REPORT & PERIOD COVERED

Technical Rept.

6. PERFORMING ORG. REPORT NUMBER

I-ALEX(01)-TR-75-08

7. AUTHOR(s)

Robert L. Sax

8. CONTRACT OR GRANT NUMBER(s)

F08606-75-C-0029
ARPA Order-2551

9. PERFORMING ORGANIZATION NAME AND ADDRESS

Texas Instruments Incorporated
Equipment Group
Dallas, Texas 75222

10. PROGRAM ELEMENT, PROJECT, TASK AREA & WORK UNIT NUMBERS

VELA T/5705/B/ETR

11. CONTROLLING OFFICE NAME AND ADDRESS

Advanced Research Projects Agency
Nuclear Monitoring Research Office
Arlington, Virginia 22209

12. REPORT DATE

31 July 1975

13. NUMBER OF PAGES

54

14. MONITORING AGENCY NAME & ADDRESS (if different from Controlling Office)

Air Force Technical Applications Center
VELA Seismological Center
Alexandria, Virginia 22314

15. SECURITY CLASS. (of this report)

UNCLASSIFIED

15a. DECLASSIFICATION/DOWNGRADING SCHEDULE

16. DISTRIBUTION STATEMENT (of this Report)

APPROVED FOR PUBLIC RELEASE, DISTRIBUTION UNLIMITED

17. DISTRIBUTION STATEMENT (of the abstract entered in Block 20, if different from Report)

18. SUPPLEMENTARY NOTES

ARPA Order No. 2551

19. KEY WORDS (Continue on reverse side if necessary and identify by block number)

Seismology	Dislocation	Discrimination
Displacement amplitude	Radiated seismic energy	
Corner frequency	Magnitude	
Source dimension	Maximum entropy spectra	

20. ABSTRACT (Continue on reverse side if necessary and identify by block number)

A method was developed for computing the displacement spectrum of earthquake dislocations and presumed explosions with greater accuracy. Measurements of corner frequencies and displacement amplitudes are considerably less ambiguous than those derived from conventional spectra. The relatively narrowband system response is apparently correctly accounted for in the equations for ground displacement, so that the displacement

OVER

DD FORM 1 JAN 73 1473 EDITION OF 1 NOV 65 IS OBSOLETE

405076

UNCLASSIFIED

SECURITY CLASSIFICATION OF THIS PAGE (When Data Entered)

20. continued

spectra are in principal valid up to 10 Hz. Presently, roundoff errors compounded by estimation errors due to the coda of the events limit the accuracy and validity of spectra at low frequencies less than approximately 1 Hz. It is anticipated that with further development of the method, valid displacement spectra can be measured at lower frequencies.

Discriminants between earthquakes and explosions were derived from measurements of corner frequency and displacement amplitudes taken from the spectra of events. These discriminants appeared to be at least as effective as other short-period spectral discriminants such as spectral splitting, spectral moments, and spectral magnitudes. The discriminants utilized measurements of spectra which are accurate only at frequencies greater than 1 Hz. Additional discriminants based on low frequency characteristics of the displacement spectra may be possible in the future when the accuracy of displacement spectral calculation is improved.

The spectral measurements of corner frequencies and displacement amplitude were used to compute magnitudes assuming $E^{1/2}$ scaling, where E is the radiated seismic energy. Comparison of spectral measurements of magnitudes at regional distances to teleseismic time domain measurements of earthquake magnitudes by the seismic network indicates that such measurements could be made with unexpected precision (approximately 0.17 standard deviations of magnitude). The results from teleseismic measurements of P-waves were less precise (approximately 0.29 standard deviations). For earthquakes, magnitudes derived from spectral parameters are consistent with the event m_b derived from time domain measurements. For explosions, magnitudes derived from spectral parameters are consistently higher than those derived from time domain measurements by a constant amount. This constant positive difference between the spectral and time domain magnitude measurement indicates events with greater high frequency radiated energy. This magnitude difference along with measurement of the spectrum corner frequency appears to be the best means of discriminating explosions from earthquakes based on the high frequency characteristics of the events.

ABSTRACT

A method was developed for computing the displacement spectrum of earthquake dislocations and presumed explosions with greater accuracy. Measurements of corner frequencies and displacement amplitudes are considerably less ambiguous than those derived from conventional spectra. The relatively narrowband system response is apparently correctly accounted for in the equations for ground displacement, so that the displacement spectra are in principal valid up to 10 Hz. Presently, roundoff errors compounded by estimation errors due to the coda of the events limit the accuracy and validity of spectra at low frequencies less than approximately 1 Hz. It is anticipated that with further development of the method, valid displacement spectra can be measured at lower frequencies.

Discriminants between earthquakes and explosions were derived from measurements of corner frequency and displacement amplitudes taken from the spectra of events. These discriminants appeared to be at least as effective as other short-period spectral discriminants such as spectral splitting, spectral moments, and spectral magnitudes. The discriminants utilized measurements of spectra which are accurate only at frequencies greater than 1 Hz. Additional discriminants based on low frequency characteristics of the displacement spectra may be possible in the future when the accuracy of displacement spectral calculation is improved.

The spectral measurements of corner frequencies and displacement amplitude were used to compute magnitudes assuming $E^{1/2}$ scaling, where E is the radiated seismic energy. Comparison of spectral measurements of magnitudes at regional distances to teleseismic time domain measurements of earthquake magnitudes by the seismic network indicates that

such measurements could be made with unexpected precision (approximately 0.17 standard deviations of magnitude). The results from teleseismic measurements of P-waves were less precise (approximately 0.29 standard deviations). For earthquakes, magnitudes derived from spectral parameters are consistent with the event m_b derived from time domain measurements. For explosions, magnitudes derived from spectral parameters are consistently higher than those derived from time domain measurements by a constant amount. This constant positive difference between the spectral and time domain magnitude measurement indicates events with greater high frequency radiated energy. This magnitude difference along with measurement of the spectrum corner frequency appears to be the best means of discriminating explosions from earthquakes based on the high frequency characteristics of the events.

ACKNOWLEDGMENTS

I greatfully acknowledge David G. Lambert and Frode Ringdal for providing the data base of NORSAR data. I received considerable assistance from Ruud Unger in the preparation of tables describing the data base and in preparation of the data and spectral plots. Many helpful suggestions and considerable editing by Stephen S. Lane are included in this report.

TABLE OF CONTENTS

LIST OF FIGURES

LIST OF FIGURES
(continued)

LIST OF TABLES

SECTION I
INTRODUCTION

The purpose of this study is to further investigate a possibility of deriving more effective short-period seismic discriminants. In the past, short-period discriminants have been used to confirm discrimination results of more reliable methods such as M_s versus m_b and focal depth estimates. An effective set of short-period discriminants would be useful in its own right. The detection capability for short period data is in most cases better than for long-period data. Also, the cost of installation and operation of a world-wide system for acquisition of long-period data is considerably greater than that for short-period data. Therefore, it is worth directing research toward establishing the limit of applying short-period data to discriminating explosions from earthquakes. Knowledge of this limit will assure that the final system configuration implemented will provide the most cost effective seismic monitoring of nuclear explosions.

SECTION II

THEORETICAL BACKGROUND AND PREVIOUS EXPERIMENTAL RESULTS

A. THEORETICAL BACKGROUND

Briefly described is a theoretical basis for applying measurements of corner frequency and other spectral parameters to the problem of discriminating between explosions and earthquakes. Brune (1970) presented a model for the spectrum of shear waves from a dislocation. His formula for the average spectrum is:

$$\langle \Omega(f) \rangle = \langle R_{\theta\phi} \rangle \frac{\sigma\beta}{\mu} F(\epsilon) \frac{1/f_c^2}{1+(f/f_c)^2} \qquad \text{(II-1)}$$

where $F(\epsilon) = \left\{ \left[2-2\epsilon \right] \left[1-\cos(1.21\,\epsilon\, f/f_c) \right] + \epsilon^2 \right\}^{1/2}$

and

σ = stress

β = shear velocity

μ = rigidity

f_c = corner frequency

ϵ = fractional stress drop

f_o = higher corner frequency due to effect of fractional stress drop

$\langle R_{\theta\phi} \rangle$ = average of radiation pattern of shear waves.

Figure II-1 shows a spectrum calculated according to Equation II-1.

If the stress drop from a dislocation is 100% complete, $\epsilon = 1$. Then the spectrum is flat nearly up to the corner frequency (f_c) and falls off as f^{-2} above the corner frequency. For $\epsilon \ll 1$, the spectrum is flat up the corner frequency above which it falls off as f^{-1}. At higher frequencies its slope gradually increases until at frequencies greater than $f_o = f_c/\epsilon$, the

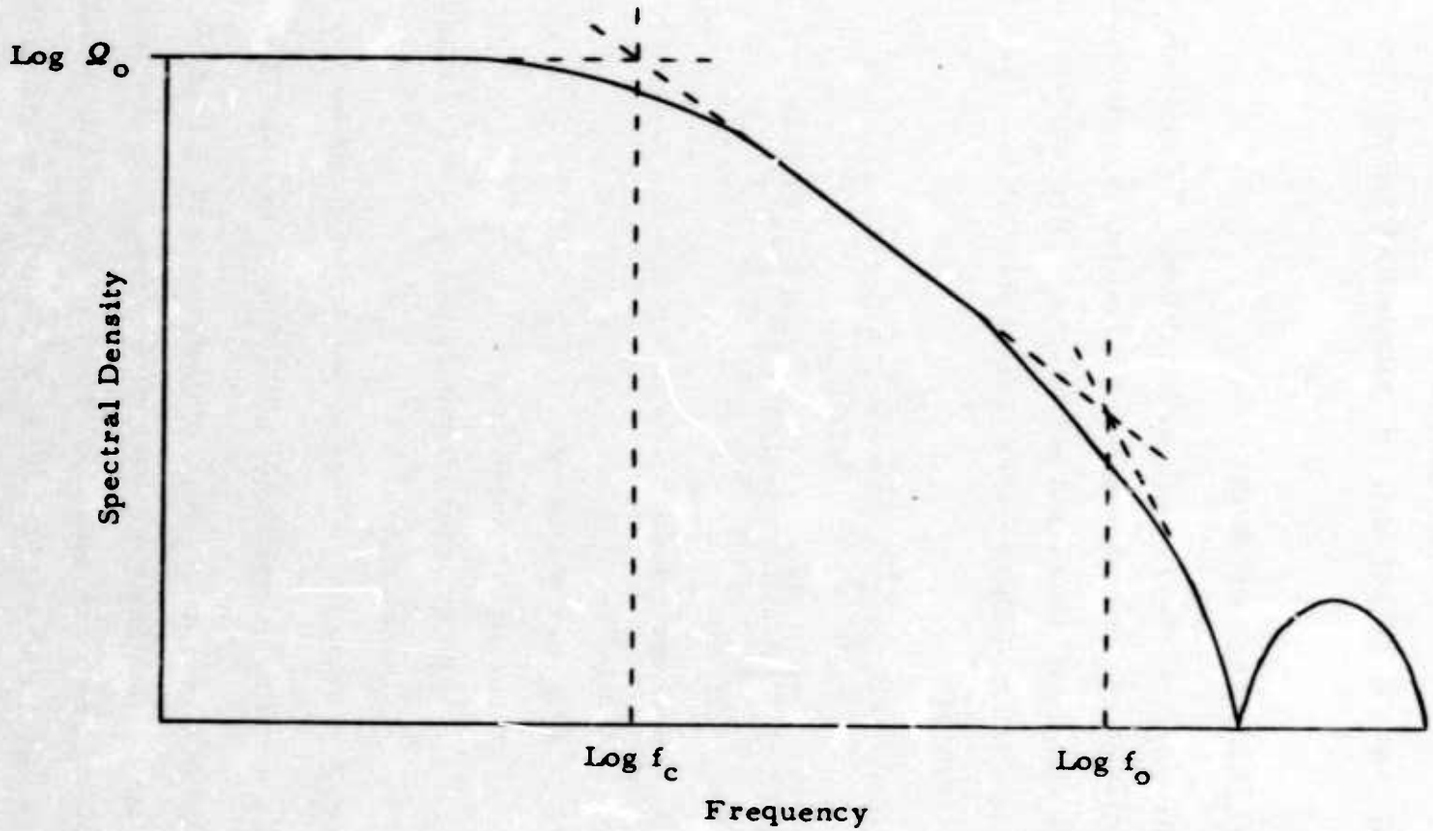

FIGURE II-1

SCHEMATIC DISPLACEMENT SPECTRAL DENSITY OF AN EARTHQUAKE WITH FRACTIONAL STRESS DROP

spectrum falls off very sharply as $f^{-\gamma_o}$ $(2<\gamma_o<10)$, as a side lobe of $F(\epsilon)$ is approached.

Hanks and Wyss (1972) presented the theoretical spectrum of P waves from an earthquake. The functional form of their result is similar to that of Brune although the definition of some parameters such as f_c and $\langle R_{\theta\phi} \rangle$ is different.

The expression for the radiated energy from earthquakes is (Hanks and Wyss 1972).

$$E_s \sim 4\pi^2 \int_{-\infty}^{\infty} \left| \Omega(f)\, f \right|^2 df \qquad \text{(II-2)}$$

by a straight forward application of Parseval's theorem to the volume integration of kinetic energy density. Equation II-2 is valid for shear or compressional waves under any model. For Brune's model, given an arbitrary exponent $-\gamma$ on the frequency above the corner frequency f_c, the radiated energy of P or S waves is given by choosing the appropriate factors in:

$$E_s(P,S) = \frac{I(P,S)}{2} \cdot (\alpha,\beta) \cdot$$

$$\rho R^2 (2\pi)^2 \frac{\Omega_o(P,S)}{\langle R^2_{\theta\phi}(P,S) \rangle} f_c^3(P,S) \left(\frac{1}{3} + \frac{1}{2\gamma - 3}\right) . \qquad \text{(II-3)}$$

Here

$I(P)$	$= 4\pi/15$, $I(S) = 2\pi/15$
(α,β)	= compressional velocity or shear velocity
R	= the distance in kilometers
ρ	= is the density.

By equating the energy derived empirically by integrating the spectra to that derived in Equation (II-3) it is possible to solve for an

"energy" corner frequency, f_e. This is an alternative method of measuring corner frequency which involves not only the corner frequency f_c but also other details of the spectrum. Assuming $\gamma = 2$ we can solve (II-3) for the energy corner frequency for P waves.

$$\text{Log } f_e = .03 + \frac{1}{3} \text{ Log} \left[\int_0^\infty \left| \Omega_n (f) \, f \right|^2 df \right]. \qquad \text{(II-4)}$$

The constant .03 was obtained using 3.32 for the density and Ω_n is the normalized amplitude spectral density taken as 1.0 below the measured corner frequency.

Another theoretical scaling law found by Thatcher and Hanks (1970) is:

$$\text{Log } (2r) = \frac{2}{3} M_L + 2.9 - \frac{2}{3} \text{ Log } \Delta\sigma$$

where $\Delta\sigma$ is the stress drop and r is the radius of the dislocation. The relationship for stress drop, where Ω_o' is corrected for attenuation, and f_c is the corner frequency in Brune's model, is:

$$\text{Log } \Delta\sigma = \text{Log } \Omega_o' + 3 \text{ Log } f_c + \text{constant.}$$

Assuming that m_b and M_L scale similarly with energy, we have

$$\text{Log } (2r) = \frac{2}{3} m_b - \frac{2}{3} \text{ Log } \Omega_o' - 2 \text{ Log } f_c + \text{constant} \qquad \text{(II-5)}$$

where m_b is a network magnitude. By taking the constant equal to zero, Log (2r) is proportional to the source dimension.

As a result of the response of the seismic system, a layered earth and absorption, the conventional magnitude probably reflects the seismic source wavelet at frequencies between 0.7 and 1.5 Hz. Thus elevated spectral magnitudes (or radiated seismic energies) reflect the combined effect of higher corner frequencies and high frequency peaks in the spectrum of the signal. The presence of the latter, although indicated by the spectra of some events, cannot be considered well established due to the present accuracy of conventional spectral computations at frequencies less than the order of 1 Hz.

B. PREVIOUS EXPERIMENTAL RESULTS

Using a data base of 136 local California events observed by a local network of seismometers, Thatcher and Hanks (1973) computed local magnitude and other source parameters from measurements of the long-period spectral displacement amplitude Ω_o and the corner frequency f_c of shear waves from local events. Their emperical scaling law was :

$$M_L = \log \Omega_o + \frac{3}{2} \log f_c + 7.2 .$$

This result combined with radiated energy computed from Equation II-4 led to the following relationship between radiated energy and M_L with good correspondence with the observed data :

$$\text{Log } E_s = 2.0\, M_L + 8.0 .$$

The local magnitude is seen to be proportional to log $E^{1/2}$.

Following these results, it has been assumed here that m_b's for regional and teleseismic events can also be estimated from measurements of Ω_o corrected for attenuation with distance and f_c, and are also proportional to log $(E_s^{1/2})$. That is:

$$m_{bs} = \log \Omega_o + \frac{3}{2} \log f_c + \text{constant} . \qquad \text{(II-7)}$$

Analysis of data by Richter (1958) shows that this assumption is close if not

exact. The validity of the assumption can also be assessed by the results obtained here.

SECTION III
SPECTRAL ESTIMATION TECHNIQUES

A. THEORETICAL DEVELOPMENT

Several methods can be used to find the earth displacement spectral density. The conventional method is to compute the power as a function of frequency using the discrete Fourier transorm, (DFT) on sampled data and to smooth the result.

There can be problems in interpreting the results of spectra computed this way. In particular, this method implictly assumes that the data outside the transform interval are zero, which is a less reasonable assumption for lower signal to noise ratios. Also, due to truncation of the signal, leakage occurs from the spectral estimate at one frequency into other f e-quencies of lower power. These effects cause large errors of unknown magnitude. For seismic data these problems are intensified by the fading random character of the recorded signal, and such errors are magnified at low frequencies when corrections are applied for the system response.

The seismic signal can be conceived of as a deterministic wavelet convolved with a random function representing multiple delayed sources, multiple paths through the medium, and reverberations due to scattering. Even direct transmissions arriving after the first can change in shape due to effects of propagation. Thus, there can be expected large varience from the assumption of time stationarity of the signal waveform and the assumption of a stationary random process for coda amplitudes. To obtain the most efficient and accurate statistical estimate of the signal which contains source effects alone it is useful to estimate the average wavelet

corresponding to the widest possible range of emergence angle from the source and paths through the medium. To obtain this result, the maximum entropy method uses the empirical autocorrelation function as input data. It computes from a large sample of data the smallest possible number of points needed to represent the average seismic signal.

The maximum entropy method (Barnard, 1969) uses a specified number of lags of the autocorrelation function ϕ as input data, and computes the best prediction error filter $\underline{\Gamma}$ in a least squares sense.

$$\left[\phi\right]\underline{\Gamma} = \underline{E} \qquad \underline{E}^t = \left[E_o\ ,\ 0,\ 0\ \ldots\ 0\right]. \tag{III-1}$$

Here $\left[\phi\right]$ is the Toplitz autocorrelation function matrix

$$\left[\phi\right] = \begin{bmatrix} \phi(0) & \phi(1) & \ldots & \phi(N) \\ \phi(1) & \phi(0) & \ldots & \phi(N-1) \\ \phi(N) & \phi(N-1) & \ldots & \phi(0) \end{bmatrix} \tag{III-2}$$

and E_o is the energy of the input times series. The filter $\underline{\Gamma}$ predicts the values of ϕ outside the data interval and thus avoids the problems associated with assuming that they are zero there. Problems arising from spectral windowing are reduced to the extent that all of the values of the autocorrelation can be predicted. Furthermore, since the prediction filter is based on that part of the input which is deterministic and hence predictable, it can be used to estimate the spectrum of the seismic wavelet, as follows :

The z transform of $\underline{\Gamma}^t = \left[\gamma_1, \gamma_2 \ldots \gamma_n\right]$ is $\sum_{n=1}^{n} \gamma_n Z^n$,

and the absolute value of the spectrum obtained by setting $Z^n = e^{in\Delta t\omega}$ in the z transform is the desired amplitude spectrum. Δt is the time between sampled data points.

Another more accurate method of solving for the prediction error filter is provided by ar algorithm refered to as the Burg technique, and is described by Ulrych (1973). This method minimizes the effect of errors in the empirical correlation function by estimating the prediction error filter coeffecients directly from the data. Comparisons of the accuracy of spectra computed conventionally by the DFT and by the maximum entropy method are given by King et al. (1974).

Another formulation of the maximum entropy method was used here to compute the displacement amplitude spectrum. It can be shown that the above formulation for the prediction error filter coeffecients is an approximation even if its assumptions are satisfied. The validity of its results depend on the amount of data used to estimate the filter. The required record length to achieve specified accuracy is related to the distance of the closest roots of the z transform of the prediction error filter coeffecients from the unit circle in the z plane. The z transform of the spectrum under Brune's model can contain multiple roots just inside the unit circle. It is therefore preferable to obtain an exact solution for the inverse autocorrelation function, A, rather than estimating it by inverting the z transform of the prediction error filter. This is done by solving

$$\left[\phi\right]\underline{A} = \underline{Q} \qquad \underline{Q}^t = \left[0, 0, 0, , E_o \ldots, 0, 0, 0\right] \tag{III-3}$$

where $A^t = \left[a_n \ldots a_o \ldots a_n\right]$ and $a_i(z) = \gamma_i^*(z)\,\gamma_i(z)$.

It can be shown that this solution $\underline{A}$ is exact for any length of sampled data. This is true even if the poles of the z transform of the prediction error filter lie on the unit circle. To find the spectral amplitude, the cosine transform of the vector $\underline{A}$ is inverted and the square root extracted. Then E_o is found by convolving the normalized inverse autocorrelation $\underline{A}$ with the empirical autocorrelation function. By extending the convolution beyond the length of the input time series, the error associated with the prediction of the autocorrelation function at these lags can be estimated. This error is expressed

as a percentage of the value at zero lag, E_o.

Given the energy E_o and the normalized inverse autocorrelation function $\underline{A}$ the amplitude spectrum is:

$$\Omega(f) = \frac{E_o^{1/2} \Delta t}{\left|1 + 2 \sum_{n=1}^{n} 2\pi nf\Delta t \; a_n \cos 2\pi nf\right|^{1/2}} \quad (m\mu\text{-sec}) \qquad \text{(III-4)}$$

where Δt is the sample time. This spectrum pertains to that part of the empirical autocorrelation function which can be predicted. For that reason the method is limited by the presence of unpredictable coda, ambient noise, and in some cases by zeros of the system response or in the signal wavelet, especially those which lie on or near the unit circle.

Just such a problem arises when computing the displacement spectrum of seismic signals as actually recorded. The seismometer response transform can be closely represented by the ratio of polynomial z transforms P(z) /Q(Z). The poles of the system response are easily removed by multiplying the z transform of the observed signal by Q(z), which can be shown to be a stable procedure and to increase the signal to noise ratio by enhancing high frequencies. On the other hand the zeros of the system response transform at NORSAR involve a 3 rd order root on the unit circle. Their removal by synthetic division by P(z) is an unstable operation which enhances roundoff errors and greatly reduces the signal to noise ratio by enhancing low frequency energy. Therefore, the equations for the maximum entropy spectrum are modified to include the zeros of the system response as follows. A modified inverse autocorrelation function $\underline{B}$ is solved by:

$$[\phi]\underline{B} = \underline{V} \qquad V^T = E_o\left[\ldots R_1, R_0, R_1 \ldots\right]$$

$$\underline{B}^T = \left[b_n, b_{n-1}, \ldots b_0, \ldots b_{n-1}, b_n\right]$$

where $R^T = \left[\ldots R_1, R_0, R_1, \ldots \right]$ is the autocorrelation function of the system response and B^T is the inverse autocorrelation function of the earth displacement corrected for instrument response. The equation for the displacement spectrum is analogous to (III-4).

$$\Omega(f) = \frac{E_o^{1/2} \Delta t}{\left| 1 + 2 \sum_{n=1}^{n} b_n \cos 2\pi n f \Delta t \right|^{1/2}} \quad (m\mu\text{-sec}). \qquad \text{(III-5)}$$

To be as objective as possible, data windows to compute the autocorrelation function are automatically determined. The initial point of a signal gate is chosen by visual inspection of the trace. Two windows beginning there are automatically detected.

The first, called the signal window, is picked by calculating the power in a fixed length gate which moved down the signal from the initial point. The point at which this power decreased for some preassigned number of points was chosen as the end of the signal gate.

The coda gate was chosen by calculating the signal-to-noise ratio based on noise preceeding the signal and a moving signal gate as before. When this signal-to-noise ratio dropped below 2.0, the end of the coda was declared.

Spectra calculated using this detector are relatively insensitive to its parameters. This procedure minimizes the influence of varying coda lengths in the determination of the signal pulse displacement spectrum.

B. NUMERICAL TESTS OF THE METHOD

The maximum entropy spectral estimation technique was tested by representing the seismic signal as a unit spike convolved with a low-pass filter. Tests were performed by choosing a corner frequency 1.0 Hz

and roll-off of 12 dB/octave. The system response was approximated by digital filters. The computed spectrum was compared to the theoretically expected spectrum, taking into account effects of instrument response and filtering. The observed spectrum was constant at the expected level.

A second test was performed to investigate the influence of the coda on the accuracy of spectra computed in this way. The test data were constructed by convolving the above 1 Hz corner frequency signal generated by multiplying a random normal variate with mean zero and standard deviation one with a factor exp (-N/50), where N was the index of the point. Spectra for synthetic signals with various values of the ratio of signal energy to coda energy (SCR) as determined from windows picked by the automatic detector, are shown in Figure III-1. The spectra in Figure III-1 are divided by the exact theoretical solution for the signal convolved with a unit spike.

Signal to coda ratio was lowered by decreasing the spike amplitude. The calculated spectral amplitude decreases as it should. Due to the effects of the automatic detector, the expected spectral level for these tests are not exactly known. Consequently the absolute values of the spectra are not significant. The relative displacement amplitude levels do appear to approximately reflect the change in signal amplitude. Note that the shape of the spectra (divided by the expected theoretical solution for a spike) should be flat.

For SCR = 4.0 the spectrum is nearly flat as expected, except for some distortion near 0.7 Hz. This distortion is more apparent at SCR = 1.0. At SCR = 0.25, the technique finds negative spectral energy in the bands near 0.7 Hz. This is indicated by a discontinuous plot of the spectra with negative power shown as blank spaces. Note the large apparent errors in the spectra at low frequencies, especially near blank spaces.

The presence of this divergence suggests that as the coda energy dominates the pulse energy in the seismic signal the spectral estimates

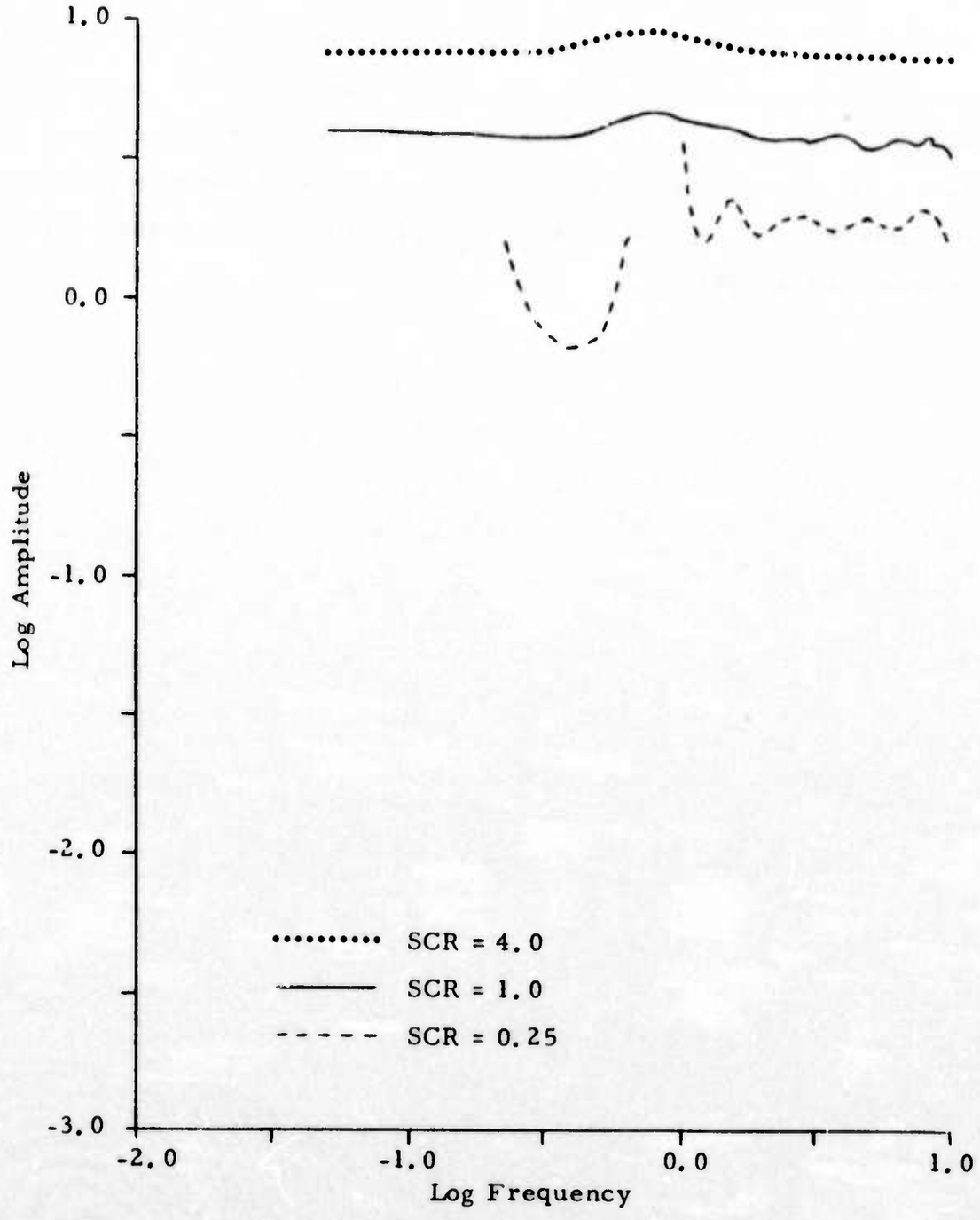

FIGURE III-1

SYNTHETIC TEST OF ERRORS DUE TO A RANDOM GAUSSIAN CODA

can be expected to become unreliable at low frequencies. Unfortunately this situation is sometimes encountered with real seismic data, and probably depends primarily on the size of the coda rather than event. As a result of these tests it is unknown whether or not our spectra are reliable at low frequencies. If reliable spectra are to be obtained at all frequencies, or at least within the widest possible frequency band, errors due to this effect must be reduced to a tolerable level.

SECTION IV
RESULTS WITH SEISMIC DATA

Twenty-eight events recorded at NORSAR are analyzed. The event parameters are listed in Table IV-1. All magnitudes are determined teleseismicly by NOAA-PDE. The data includes 6 regional earthquakes between magnitude 3.1 and 4.5; 4 teleseismic earthquakes between magnitude 5.4 and 6.1; 2 regional presumed explosions; and 8 teleseismic presumed explosions of magnitude between 4.4 and 5.6. All these signals have signal-to-noise ratios greater than 2.0.

On Figure IV-1 are earth displacement spectra of 4 teleseismic presumed explosions. Most spectra exhibit a broad peak at about 2.5 Hz and fall off sharply above corner frequencies between 3.2 and 4.8 Hz. At lower frequencies the spectra decrease in amplitude at a rate of 0 to 6 dB/octave. The effects of errors in the displacement spectrum is apparent as gaps in the spectra. These occur at frequencies where negative power was erroneously indicated. The seismometer recordings filtered to remove poles in the system response are shown with the spectra.

On Figure IV-2 are earth displacement spectra of 4 of the regional earthquakes. Corner frequencies lie between 2.2 and 4.5 Hz. Nearly constant amplitudes appear below the apparent corner frequencies. Considerable effects due to errors in calculating the ground displacement spectra are indicated by gaps in the spectra, and by large and erroneous varriations near those gaps. Data in the signal window are also shown.

Where the signal-to-noise ratio is large it is possible to compare the maximum likelihood spectra with conventional spectra computed

TABLE IV-1

EARTHQUAKE DATA BASE

	Event	Date	Origin Time	Latitude	Longitude	Depth (km)	m_b	Distance (degrees)
Regional	REQ1	09/04/72	07:00:04	67.7N	33.4E	7	4.8	11.8
	REQ2	02/28/74	22:18:49	81.6N	02.0E	--	4.5	21.0
	REQ8	04/28/74	12:52:50	68.7N	16.2E	--	4.3	8.2
	REQ9	09/19/71	11:00:07	57.8N	41.1E	--	4.5	15.5
	REQ11L	06/05/73	06:29:35	61.0N	24.0E	0	3.1	6.4
	REQ12L	07/07/73	10:51:25	60.0N	29.0E	0	3.4	9.0
	REQ13	01/24/74	09:40:16	38.3N	20.0E	33	4.5	23.3
	REQ14	01/29/74	15:12:45	38.4N	21.8E	31	4.5	23.5
	REQ15	02/23/74	01:28:46	38.1N	21.8E	37	4.0	23.8
	REQ17L	04/17/74	01:31:34	46.0N	21.1E	--	3.7	16.0
Teleseismic	TEQ1	07/02/72	12:56:07	30.1N	50.8E	31	5.4	40.5
	TEQ4	05/03/71	00:33:23	30.8N	84.5E	16	5.4	55.6
	TEQ5	09/15/71	14:55:05	39.1N	143.4E	17	5.8	72.9
	TEQ6	09/06/71	13:37:11	46.7N	141.4E	29	6.1	65.3
	TEQ7	08/29/71	15:16:56	36.5N	78.5E	--	5.0	47.9
	TEQ8	08/01/71	02:06:06	50.4N	156.8E	20	5.6	65.3
	TEQ9	06/14/72	04:36:28	33.0N	46.1E	--	5.3	35.9
	TEQ10	06/15/72	14:04:08	52.8N	160.8E	55	5.1	63.7

L = Local Determination

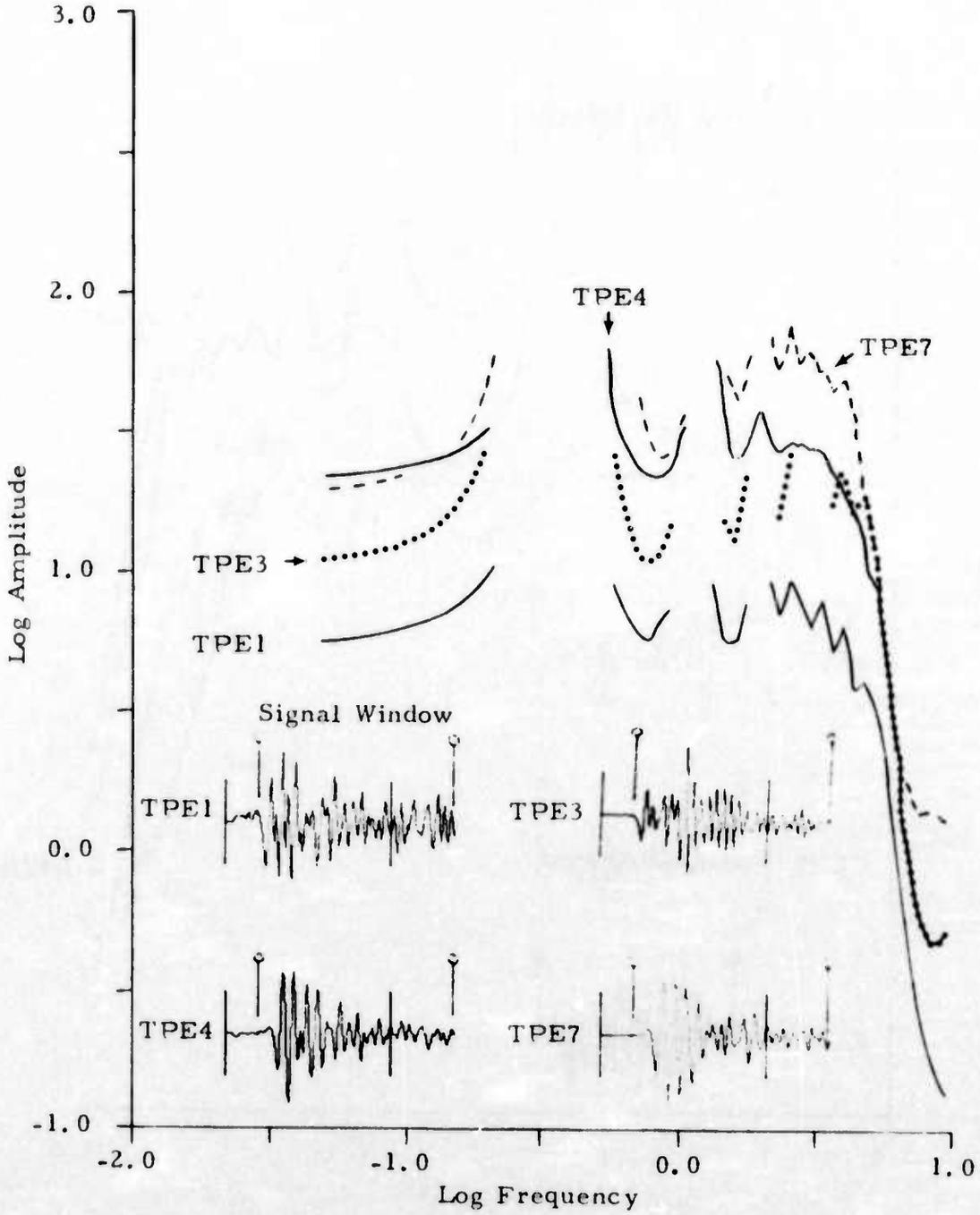

FIGURE IV-1

DISPLACEMENT SPECTRAL DENSITY OF TELESEISMIC PRESUMED EXPLOSIONS

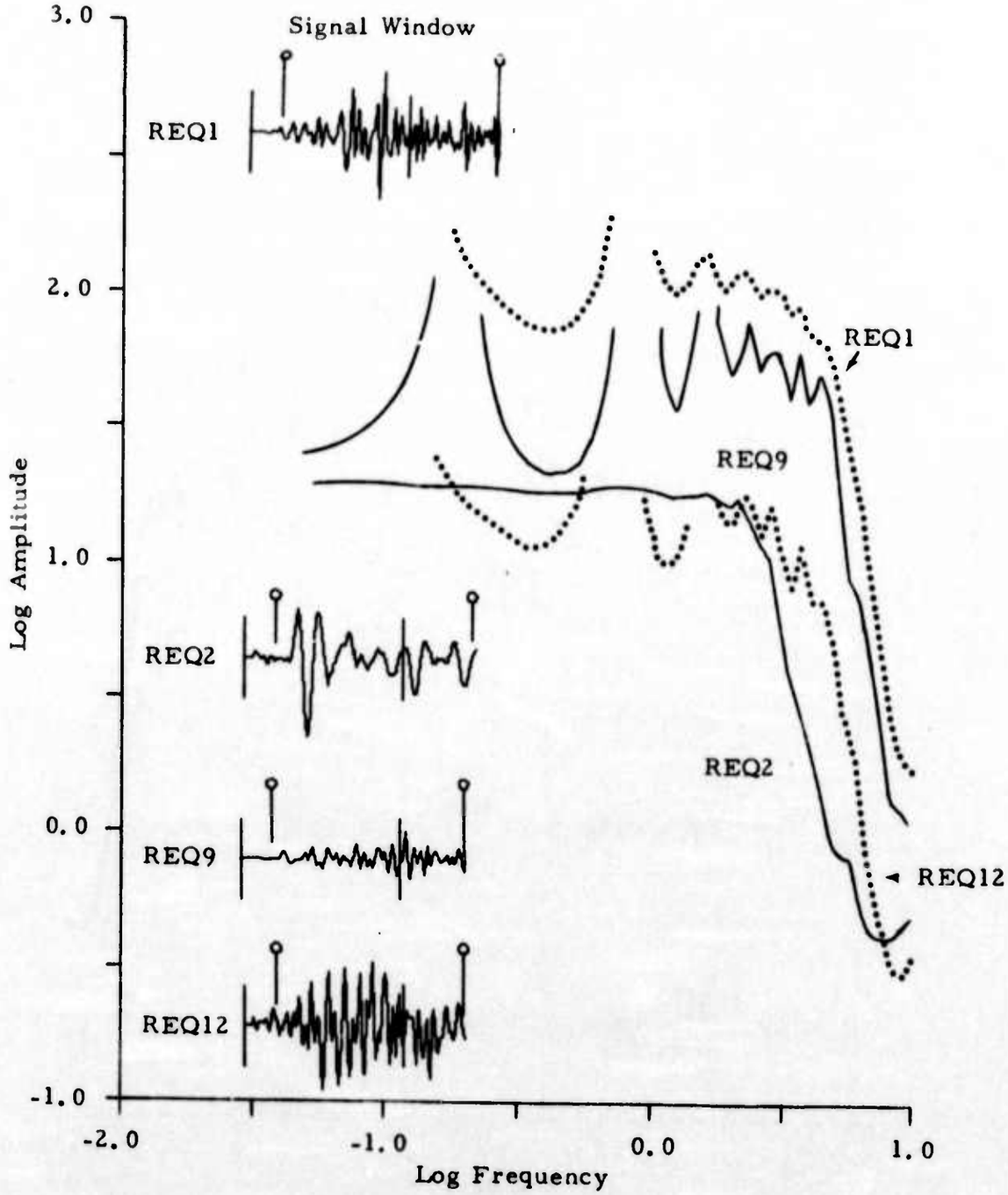

FIGURE IV-2

DISPLACEMENT SPECTRAL DENSITY
OF REGIONAL EARTHQUAKES

with 100 lags of the autocorrelation function and a Hanning window. Figure IV-3 shows such a comparison for regional earthquake REQ8; Figure IV-4 for REQ12; Figure IV-5 for REQ11; Figure IV-6 for the teleseismic presumed explosion TPE4; Figure IV-7 for TPE5; Figure IV-8 for the teleseismic earthquake TEQ6; and Figure IV-9 for TEQ4. In most cases the corner is indicated with less ambiguity by the new method. However, these are preliminary results and should be treated with caution until the effects of errors, whose presence is obvious from inspection of the results, have been resolved.

Figure IV-10 illustrates three regional earthquakes from nearly the same location in Greece. These events are gradually emergent, and amply demonstrate the ability of the automatic detector to pick the signal window.

Corner frequencies, frequency exponents, and displacement amplitudes measured from earthquake spectra are shown in Table IV-2. A test on the energy was made to check whether the measurements are representative of Brune's model.

In Brune's model, γ lies between 1.0 and 2.0, and γ_o ranges from 2.0 to 10.0, depending on the fractional stress drop. The frequency exponents shown in Table IV-2 appear to obey these requirements. Consequently the corner frequencies there were used to estimate ϵ shown on Table IV-2 through :

$$\epsilon = 0.8 \log (f_o - f_c) \qquad \text{(IV-1)}$$

which is an approximation to Brune's theoretical results.

Equation (II-4) was used to calculate an equivalent corner frequency under Brune's model by integrating the square of the spectral density to find the radiated seismic energy E_s. The calculated values of the

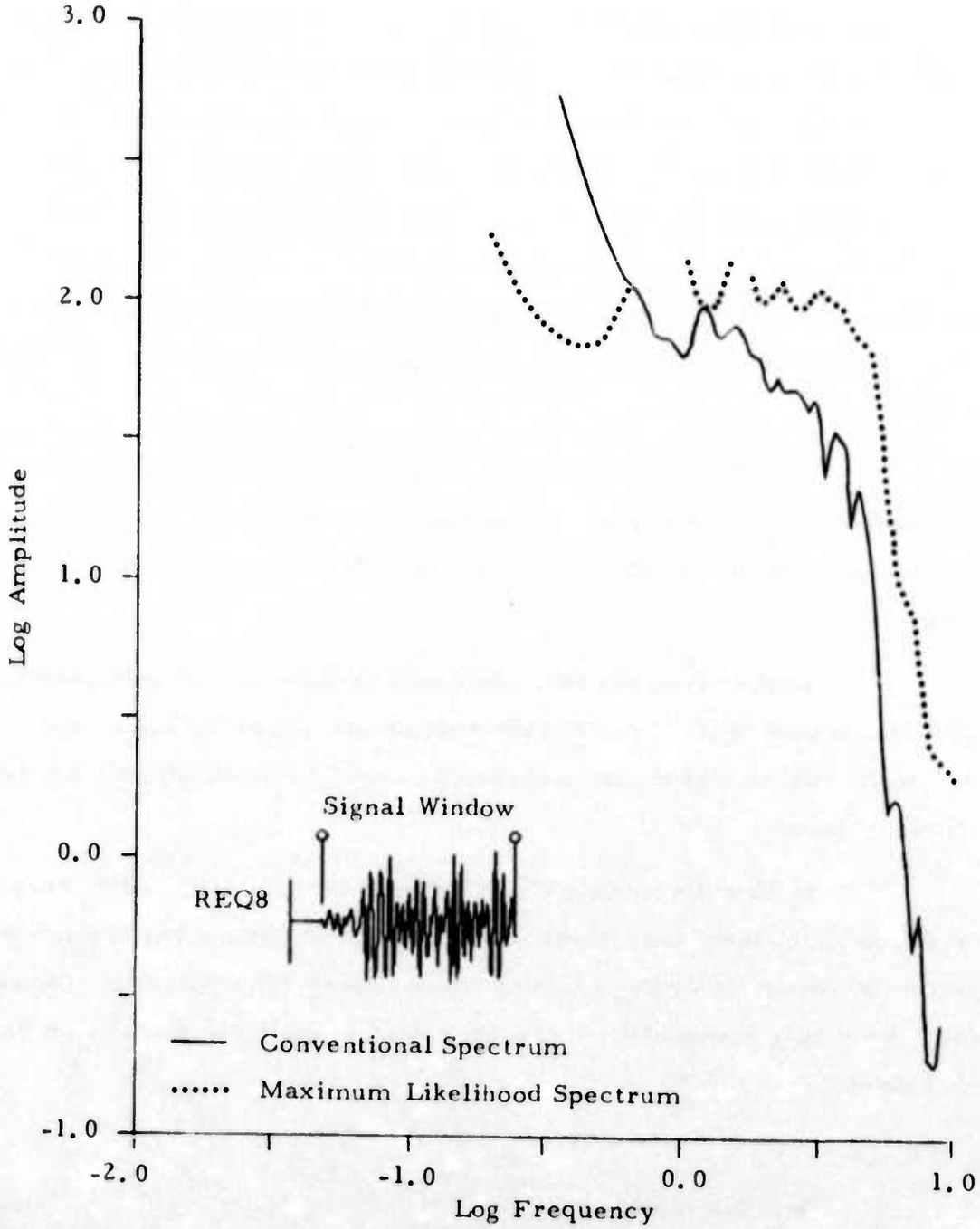

FIGURE IV-3

COMPARISON OF DFT AND MAXIMUM
ENTROPY SPECTRUM OF A REGIONAL EARTHQUAKE

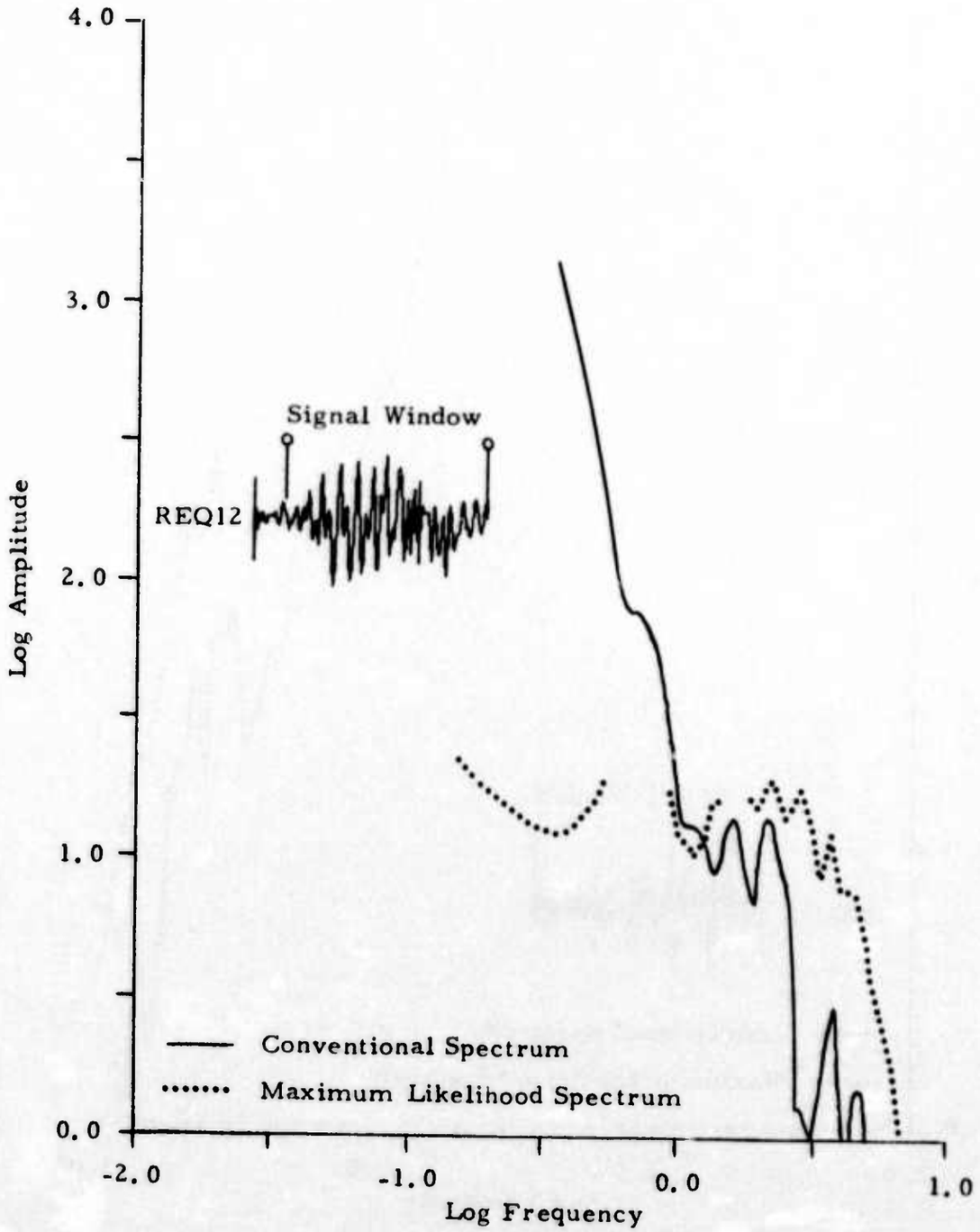

FIGURE IV-4

COMPARISON OF DFT AND MAXIMUM ENTROPY SPECTRUM OF A REGIONAL EARTHQUAKE

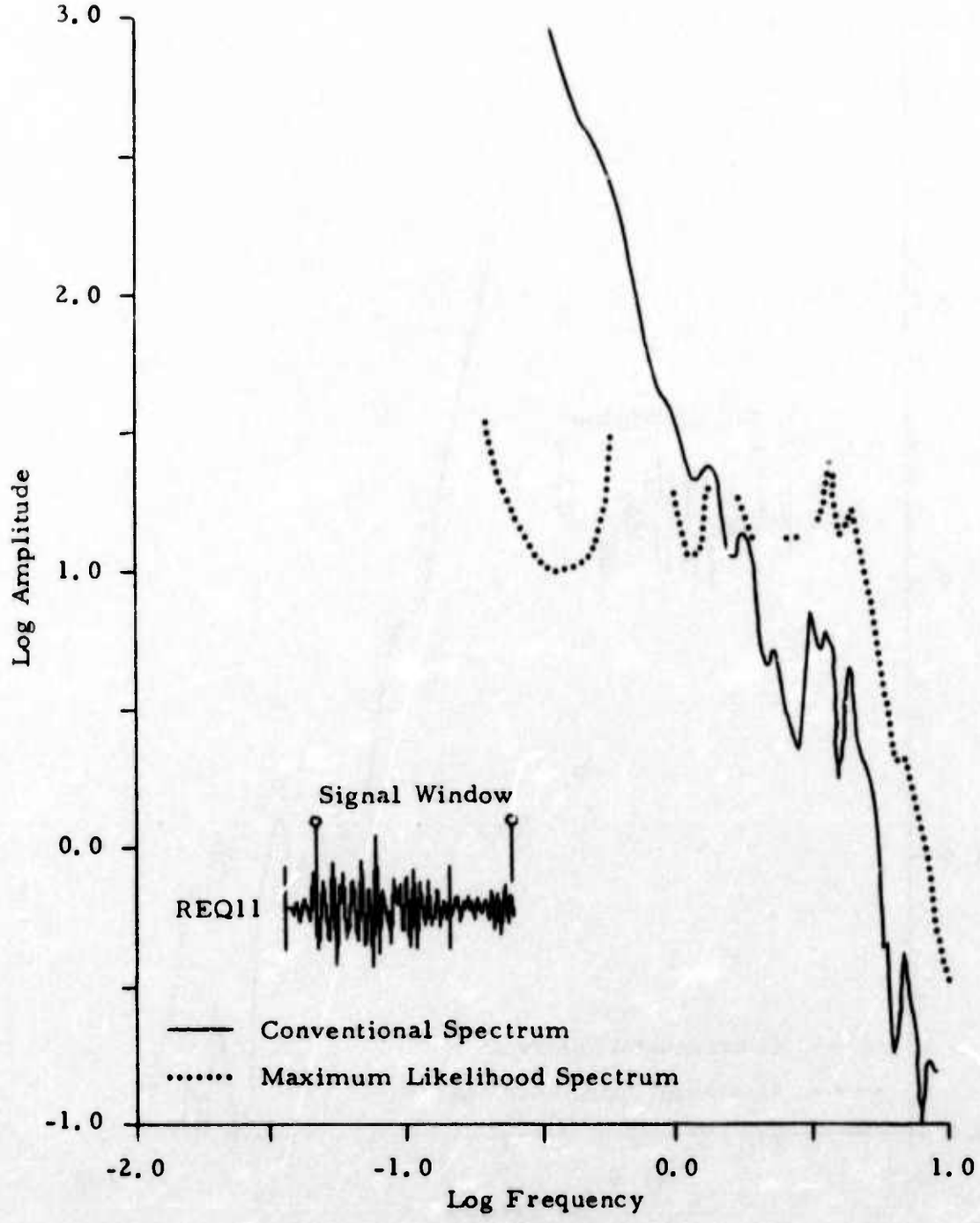

FIGURE IV-5

COMPARISON OF DFT AND MAXIMUM ENTROPY SPECTRUM OF A REGIONAL EARTHQUAKE

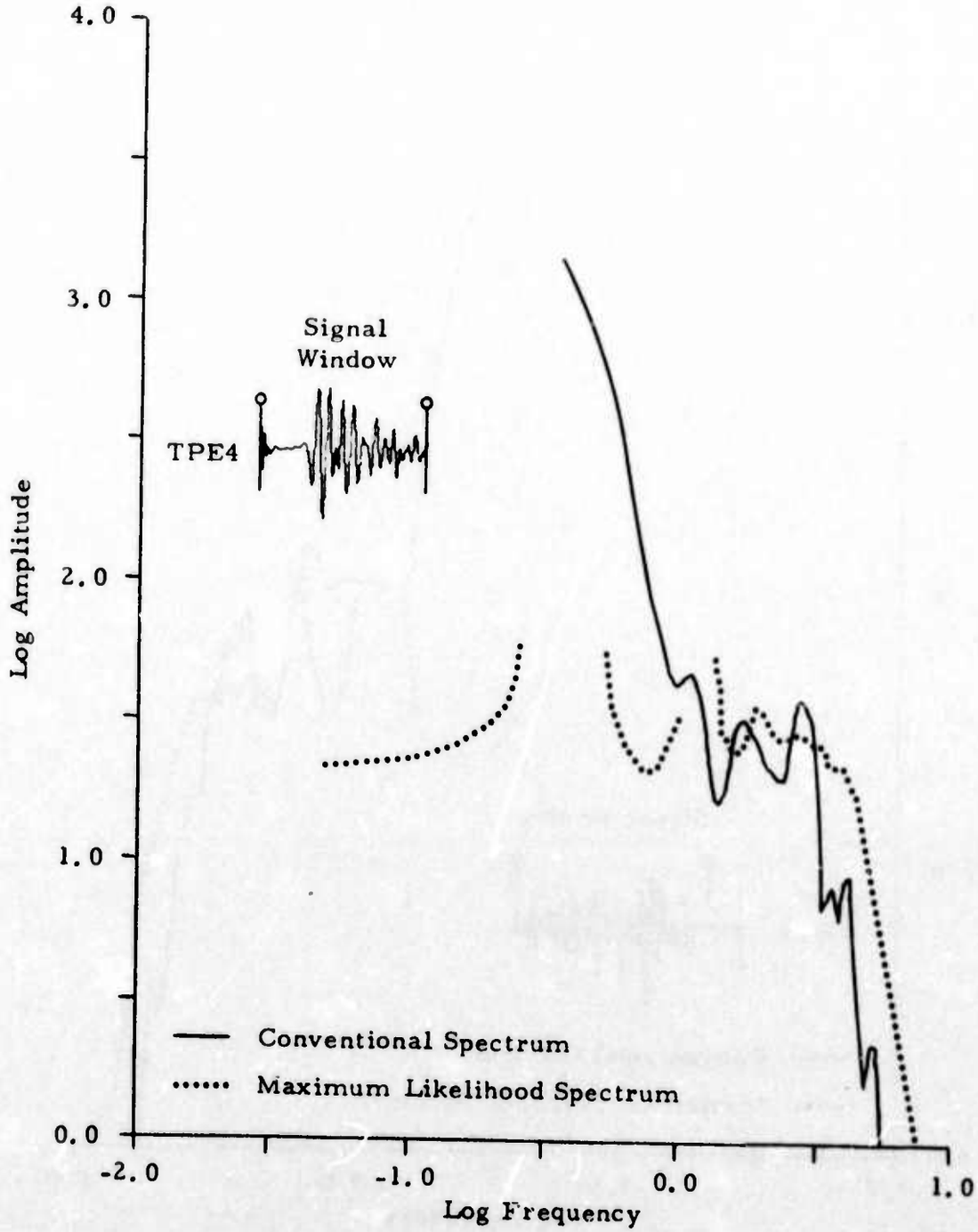

FIGURE IV-6

COMPARISON OF DFT AND MAXIMUM ENTROPY SPECTRUM OF A PRESUMED EXPLOSION

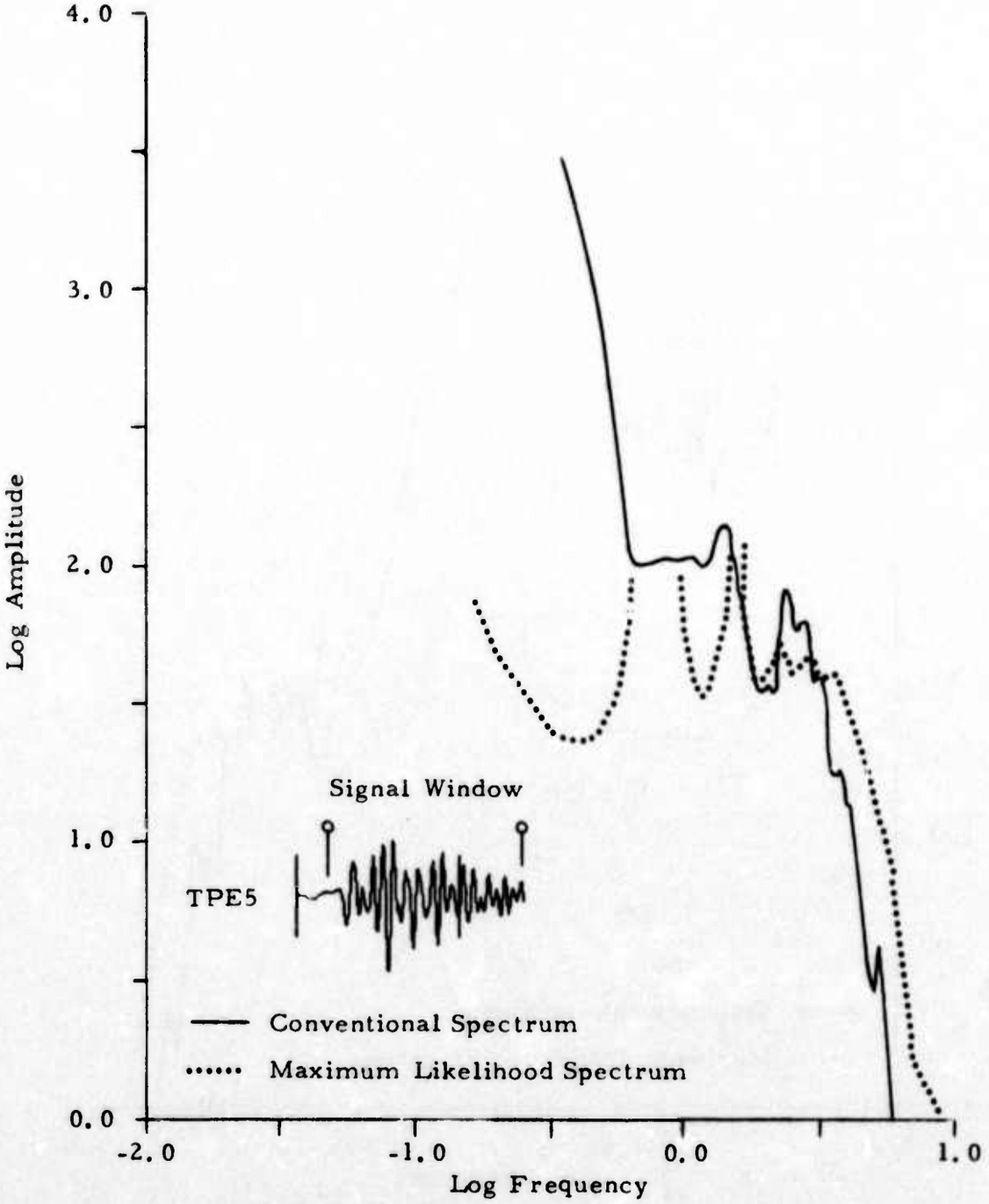

FIGURE IV-7

COMPARISON OF DFT AND MAXIMUM ENTROPY SPECTRUM OF A PRESUMED EXPLOSION

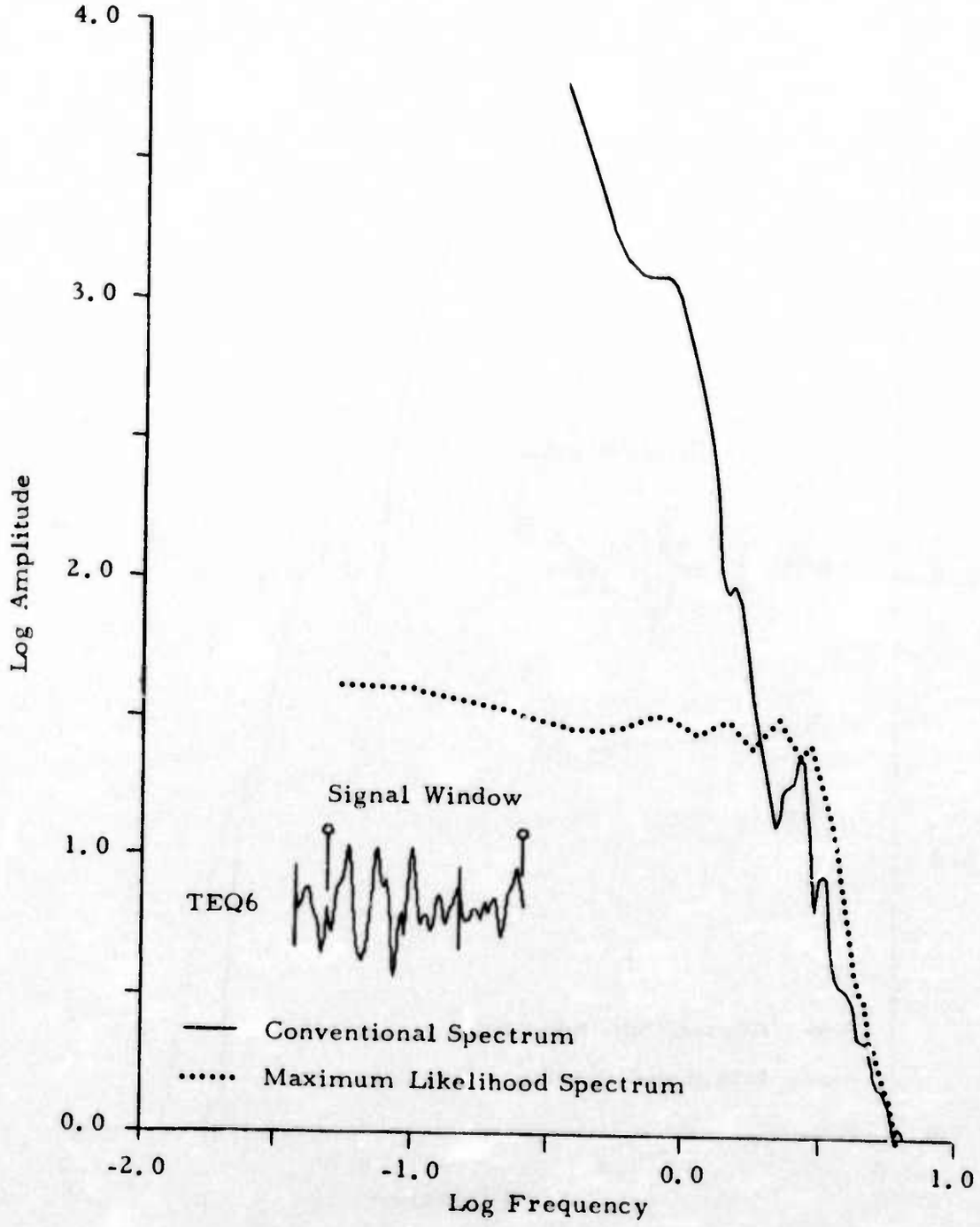

FIGURE IV-8

COMPARISON OF DFT AND MAXIMUM ENTROPY SPECTRUM OF A TELESEISMIC EARTHQUAKE

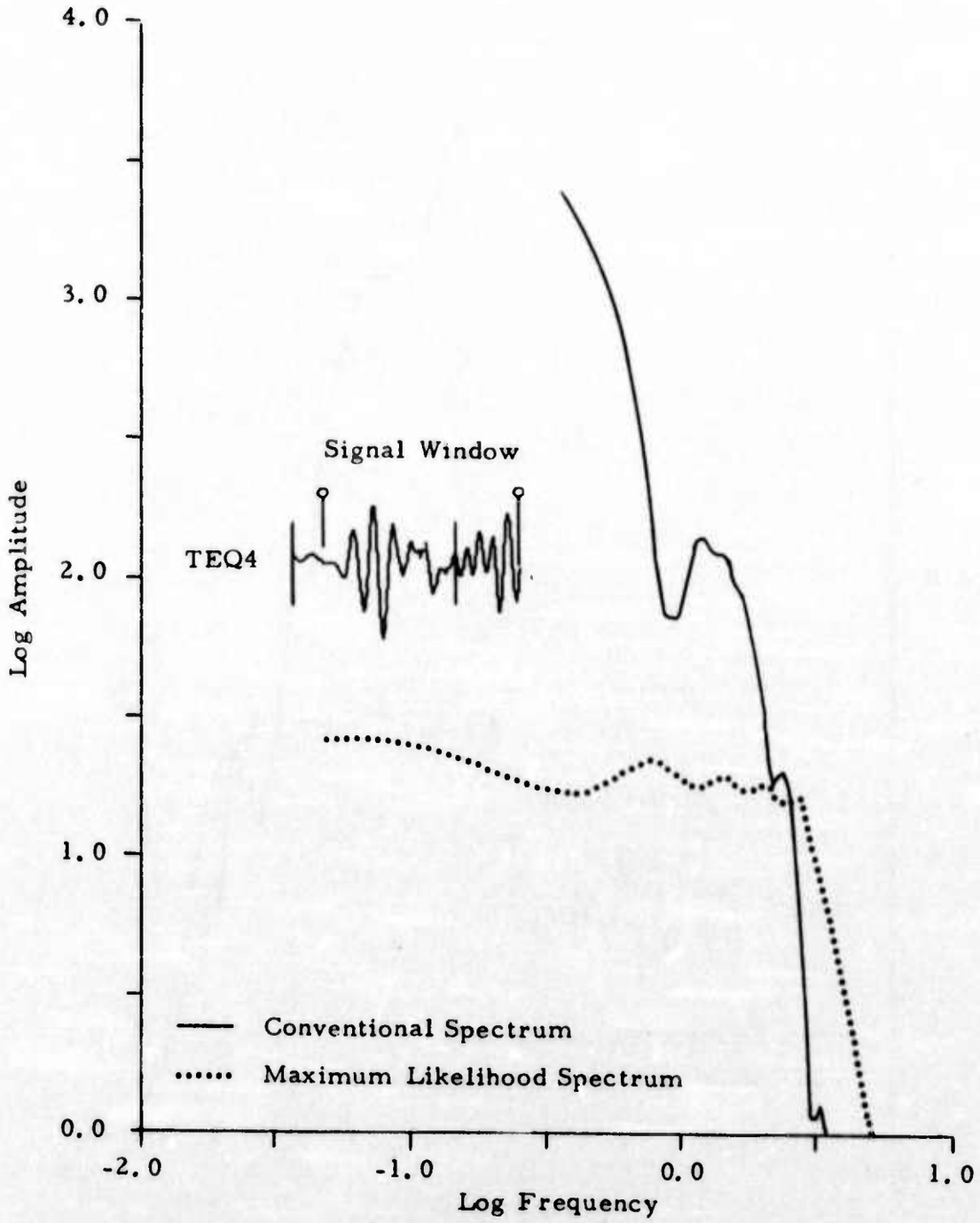

FIGURE IV-9

COMPARISON OF DFT AND MAXIMUM ENTROPY SPECTRUM OF A TELESEISMIC EARTHQUAKE

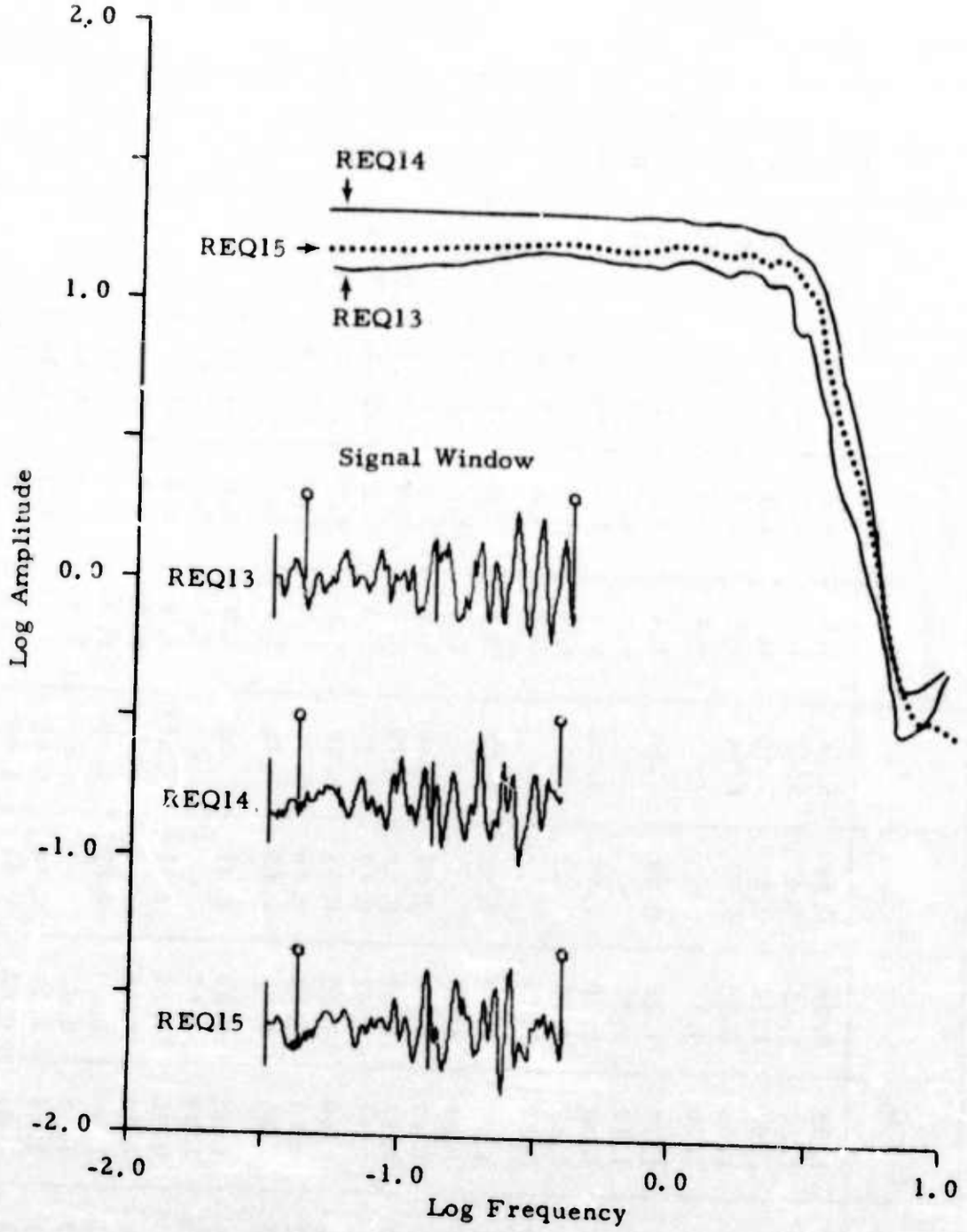

FIGURE IV-10

COMPARISON OF DFT AND MAXIMUM ENTROPY SPECTRUM OF REGIONAL EARTHQUAKES FROM GREECE

TABLE IV-2

EVENT PARAMETERS

Event	Log f_c	Log Ω_o	γ	Log f_o	γ_o	Network m_b	NORSAR Spectral m_b	Log 2r	ϵ	Log f_e
REQ1	0.48	1.98	0.88	0.66	5.44	4.8	4.5	0.18	0.71	0.48
REQ2	0.28	1.28	1.65	0.42	3.77	4.5	4.3	-0.13	0.77	0.31
REQ8	0.51	2.02	1.14	0.68	5.50	4.3	4.1	-0.40	0.73	0.55
REQ9	0.30	1.95	0.83	0.67	5.74	4.5	4.6	-0.35	0.50	0.47
REQ11	0.62	1.30	4.77	-	-	3.1	3.3	-0.59	1.00	0.55
REQ12	0.37	1.15	1.24	0.68	5.50	3.4	3.2	-0.22	0.56	0.47
REQ13	0.45	1.17	4.11	-	-	4.5	4.6	-0.49	1.00	0.39
REQ14	0.28	1.32	0.80	0.50	4.30	4.5	4.5	-0.26	0.67	0.40
REQ15	0.43	1.12	4.25	-	-	4.4	4.5	-0.50	1.00	0.37
REQ17	0.50	0.80	5.70	-	-	3.7	3.8	-0.54	1.00	0.43
TEQ1	0.32	1.22	0.93	0.67	6.27	5.4	5.2	-0.18	0.52	0.46
TEQ4	0.43	1.28	4.60	-	-	5.4	5.6	-0.54	1.00	0.36
TEQ5	0.20	1.41	2.08	0.58	4.29	5.8	5.5	0.02	0.50	0.27
TEQ6	0.40	1.47	2.09	0.51	4.79	6.1	5.8	-0.18	0.82	0.39
TEQ7	0.34	1.13	1.98	0.67	7.10	5.0	5.2	-0.44	0.54	0.38
TEQ8	0.34	1.60	2.20	0.65	8.18	5.6	5.9	-0.66	0.60	0.48
TEQ9	0.38	1.13	0.88	0.56	5.90	5.3	5.2	-0.28	0.71	0.43
TEQ10	0.37	1.16	2.03	0.68	7.76	5.1	5.4	-0.58	0.56	0.40
RPE4	0.59	1.93	3.23	0.73	7.31	4.8	5.6	-1.12		
RPE5	0.53	1.89	4.62	-	-	5.3	5.2	-0.47		
TPE1	0.40	0.90	1.34	0.72	5.68	4.4	5.0	-1.25		
TPE3	0.68	1.25	6.09	-	-	5.0	5.7	-1.17		
TPE4	0.43	1.56	0.89	0.62	4.79	5.3	5.7	-0.68		
TPE5	0.67	1.56	4.22	-	-	5.6	6.0	-0.96		
TPE6	0.51	1.66	1.71	0.68	5.61	5.4	5.9	-0.84		
TPE7	0.38	1.81	0.83	0.61	5.40	5.5	5.9	-0.61		
TPE8	0.37	2.10	1.11	0.59	4.62	5.5	6.1	-1.53		
TPE9	0.53	1.58	4.41	-	-	5.3	5.8	-0.89		

corner frequency, f_e, found from the energy, are shown in Table IV-2 and Figure IV-11. The correlation coefficent between f_e and f_c is 0.95, and the standard deviation between f_e and f_c is 0.083 Hz. Consequently we find that there is good consistency between the model and the data, and that quantities other than corner frequency and low frequency displacement amplitude can be described by the model.

Spectral magnitudes estimated by an equation analogous to equation (II-5) for local magnitude, are given by equation (IV-2).

$$m_{sb} = \log \Omega_o + 1.5 \log f_c + k \log \Delta + C. \qquad \text{(IV-2)}$$

In this equation C determined empirically for the earthquake sample by minimizing the variance between the calculated m_{sb} and m_b measured by the network. The factor k for distance scaling was taken to be +3.0 for regional events and +1.0 for teleseismic events, reflecting the presence of head waves and direct waves respectively. For the regional events, an average value of C was found to be -1.39, and the standard deviation between the magnitudes determined by equation (IV-2) using this value and the network magnitudes was 0.17 magnitude units. For the teleseismic events, C was +1.89 and the standard deviation between network and spectral magnitudes was 0.29 magnitude units. For the whole sample, the standard deviation between the two magnitude estimates was 0.20 magnitude units, and the two magnitude estimates were highly correlated with coeffecient 0.97.

An attenuation factor

$$C + k \log \Delta = m_b - \log \Omega_o - \frac{3}{2} \log f_c$$

is plotted as a function of epicentral distance in Figure IV-12 for each event

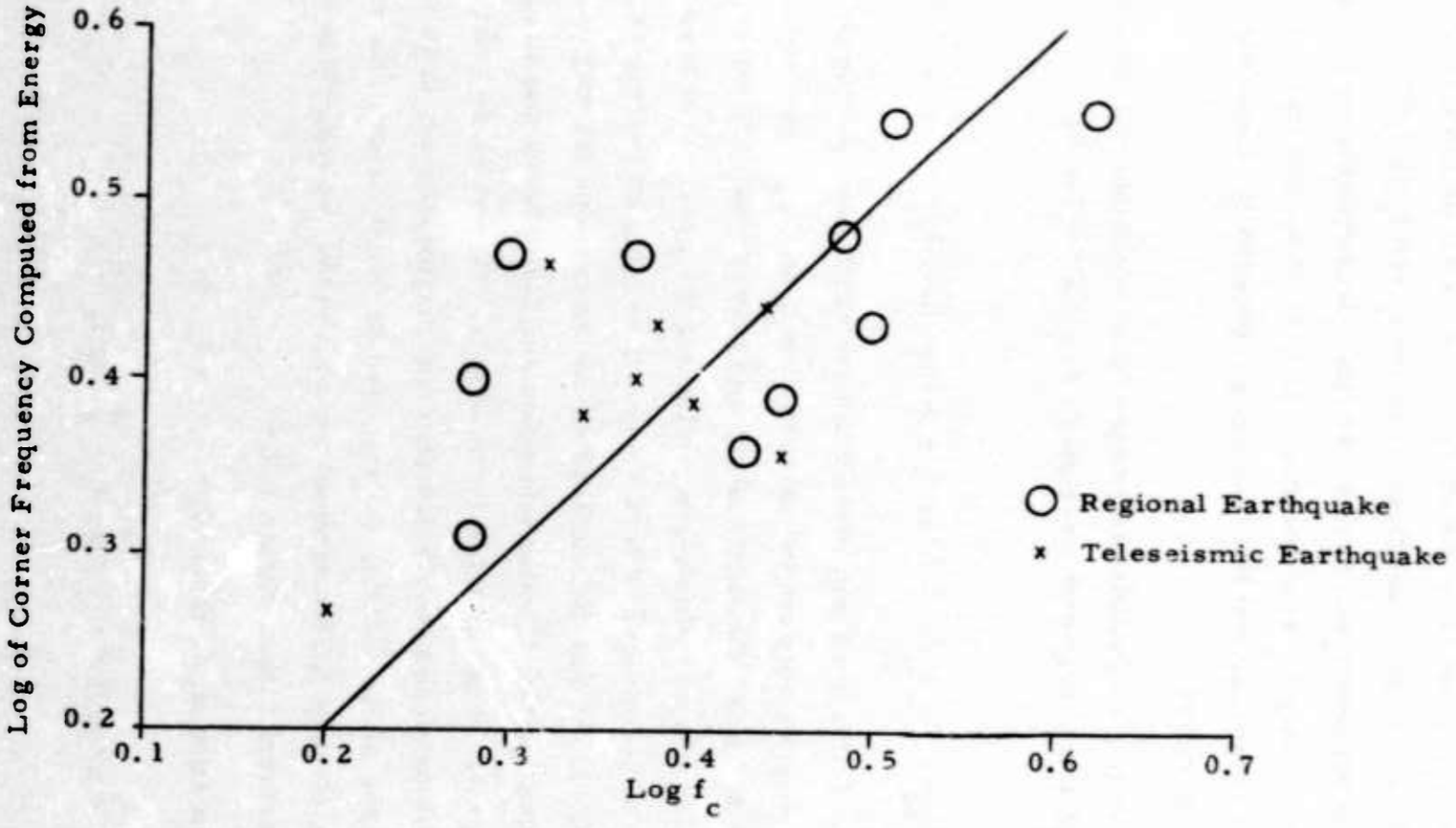

FIGURE IV-11

COMPARISON OF MEASURED CORNER FREQUENCIES WITH CORNER FREQUENCIES DERIVED FROM MEASURED RADIATED SEISMIC ENERGY AND BRUNE'S MODEL

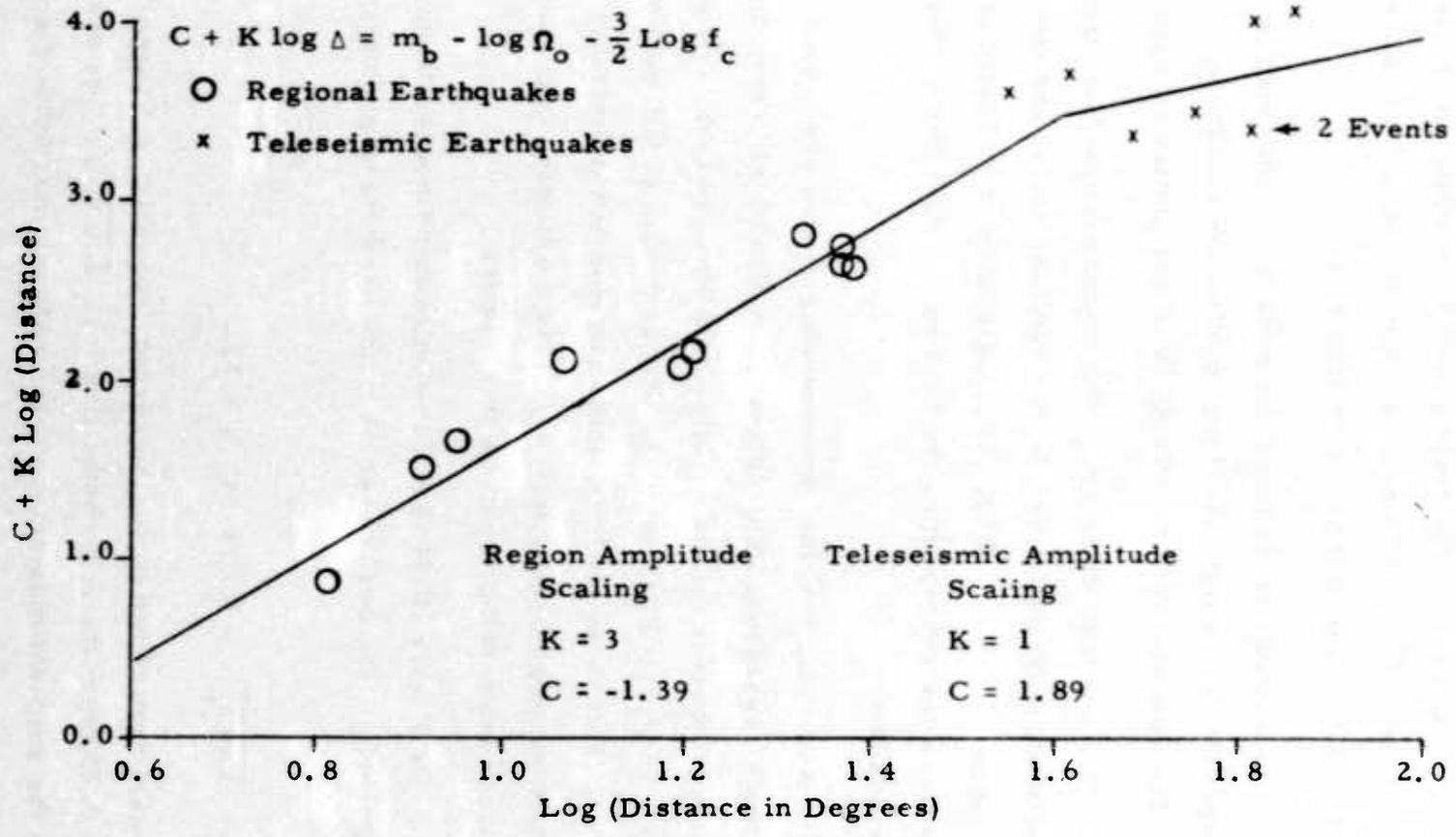

FIGURE IV-12

EMPIRICALLY DERIVED SPECTRAL AMPLITUDE SCALING WITH EPICENTRAL DISTANCE

in the earthquake sample. The solid lines are the best fit to the data, using the values of C found above. The transisition from regional to teleseismic behavior occurs at 39.8° for this data set, but only small variations in the value of C would allow this point to be shifted to 25°.

To investigate its power as a discriminant, the specral magnitude computed from equation (IV-2) was plotted for earthquakes and presumed explosions. The data are shown on Table IV-2 and plotted on Figure IV-13.

The average deviation of the explosion spectral magnitudes from their network magnitudes was 0.54 magnitude units, and their correlation with the network m_b was 0.98. This difference is reflected in the displacement of the lines representing the best linear fit to the earthquakes and presumed explosions.

Assuming that the explosion magnitudes are normally distributed about their regression line, 95% of them should fall above the dashed line. All the earthquakes fall on or below this line, and only one presumed explosion lies below it. Furthermore, that explosion is believed to be a multiple event. For these reasons, this criterion has promise as a discriminant. It should be emphasized, however, that the limited data sample prevents hard conclusions from being drawn on this subject.

On Figure IV-14 is a plot of measured corner frequencies versus network magnitude. The best linear fit to the earthquake population is

$$\overline{\text{Log } f_c} = -0.074\ m_b + 0.74. \qquad \text{(IV-3)}$$

Six of the logarithms of the explosion corner frequency measurements lie further than 0.13 from the regression line for $\overline{\text{Log } f_c}$. The event RPE5, which failed the spectral magnitude versus network magnitude discrimination test was claimed to be an explosion by this corner frequency versus network

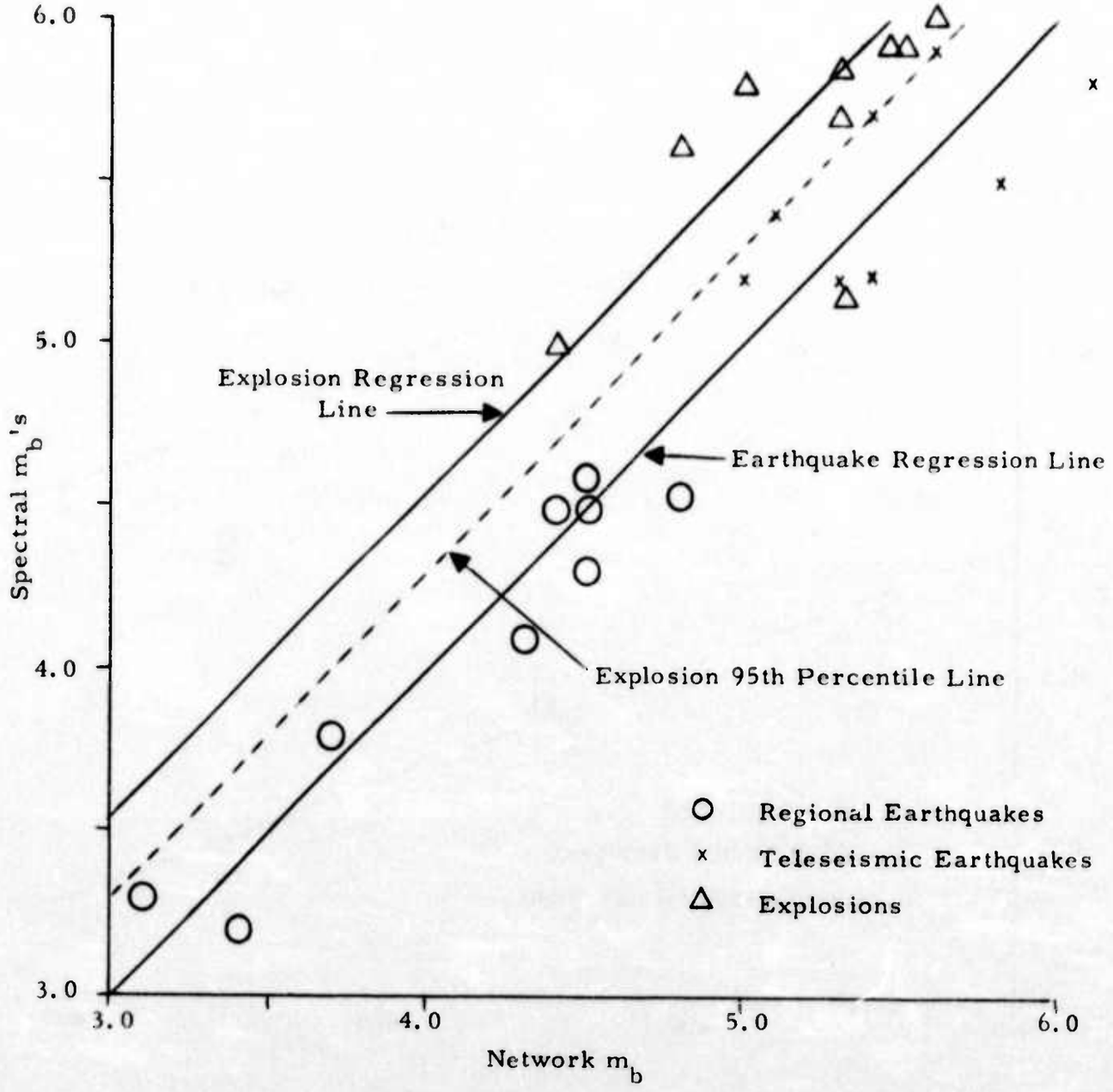

FIGURE IV-13

MAGNITUDES COMPUTED FROM SPECTRA OF NORSAR DATA m_{bs} COMPARED WITH EVENT MAGNITUDES AVERAGED FROM TELESEISMIC NOAA-PDE MEASUREMENTS OF m_b

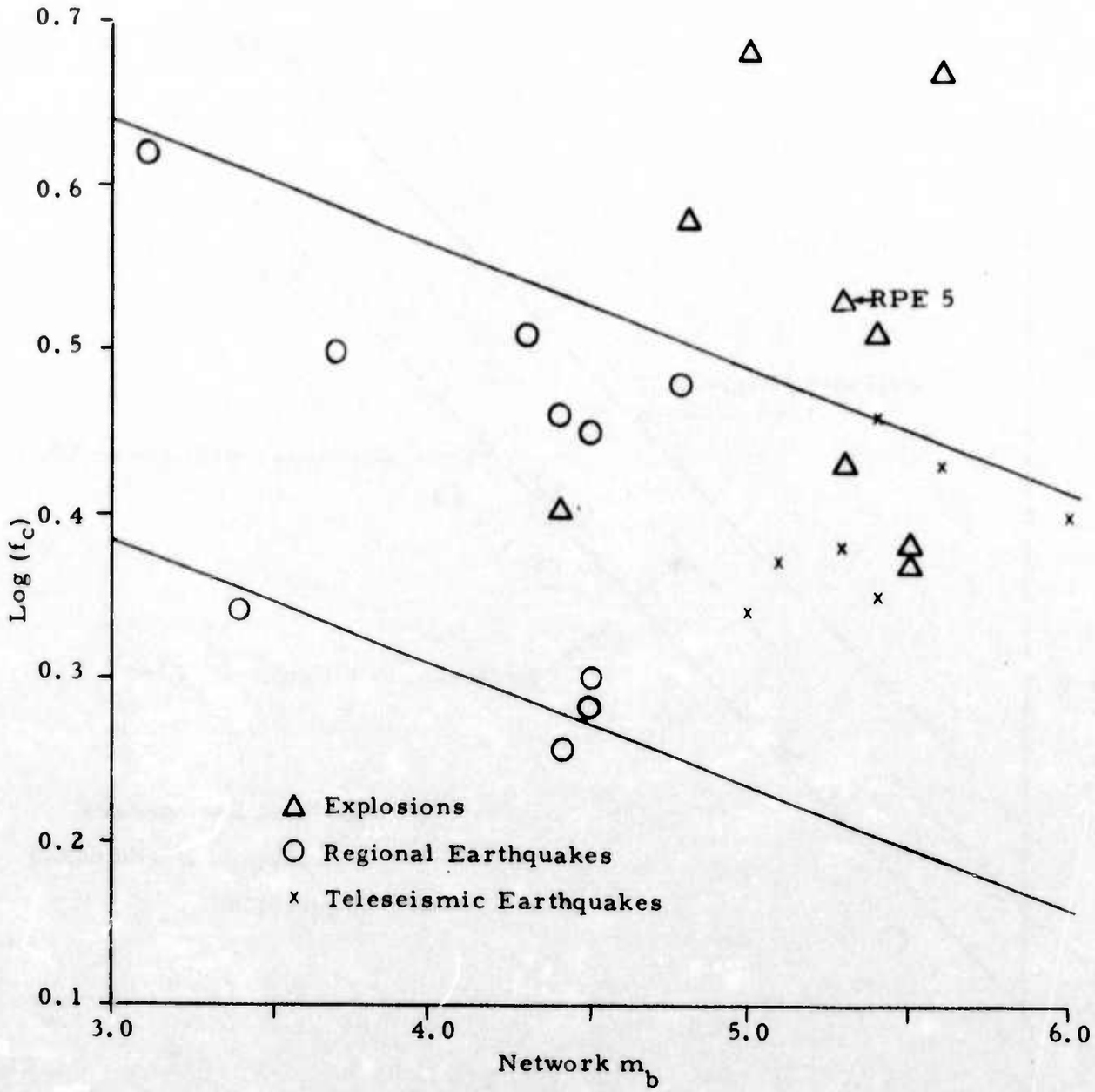

FIGURE IV-14

LOG OF THE CORNER FREQUENCY MEASUREMENTS
VERSUS NETWORK MAGNITUDE

magnitude test. The large amount of scatter evident is consistent with the results of Peppin (1967) and Thatcher and Hanks (1973).

Figure IV-15 is an empirical plot of $\text{Log}\,\Omega_o$ corrected for distance attenuation defined to be

$$\text{Log}\,\Omega_o' = \text{Log}\,\Omega_o + k\,\text{Log}\,\Delta + C \qquad \text{(IV-4)}$$

where C = -1.39 and k = 3 for regional events, and C = 1.89 and k = 1 for teleseismic events. The median line for the average $\overline{\text{Log}\,\Omega_o'}$ versus network magnitude is

$$\overline{\text{Log}\,\Omega_o'} = 1.14\,m_b - 1.21\ . \qquad \text{(IV-5)}$$

Another linear combination of $\text{Log}\,\Omega_o$ and $\text{Log}\,f_c$, which could provide discrimination information is the logarithm of the source dimension, which should be smaller for explosions than for earthquakes. From equation (II-5), Log (2r) is plotted against $\Delta m = m_{bs} - m_b$, which reflects anomalous radiated seismic energy. The results are shown on Figure IV-16, where all of the explosions are separated except RPE5. Eight of the ten explosions show well defined separation from the space occupied by earthquakes.

Where $\Delta\log f_c$ is the deviation of the logarithmic frequency from its expected value given by equation (IV-3), Figure IV-17 shows $\Delta\log f_c$ plotted against m_b. This discriminant combines those presented in Figures IV-13 and IV-14. Complete discrimination between earthquakes and explosions is obtained by the solid lines, which require that events whose corner frequency is anomolously high or whose spectral magnitude is anamolously high be classified as explosions. However, the discriminant based solely on corner frequency is supported by only one point, and further data are required to establish its validity.

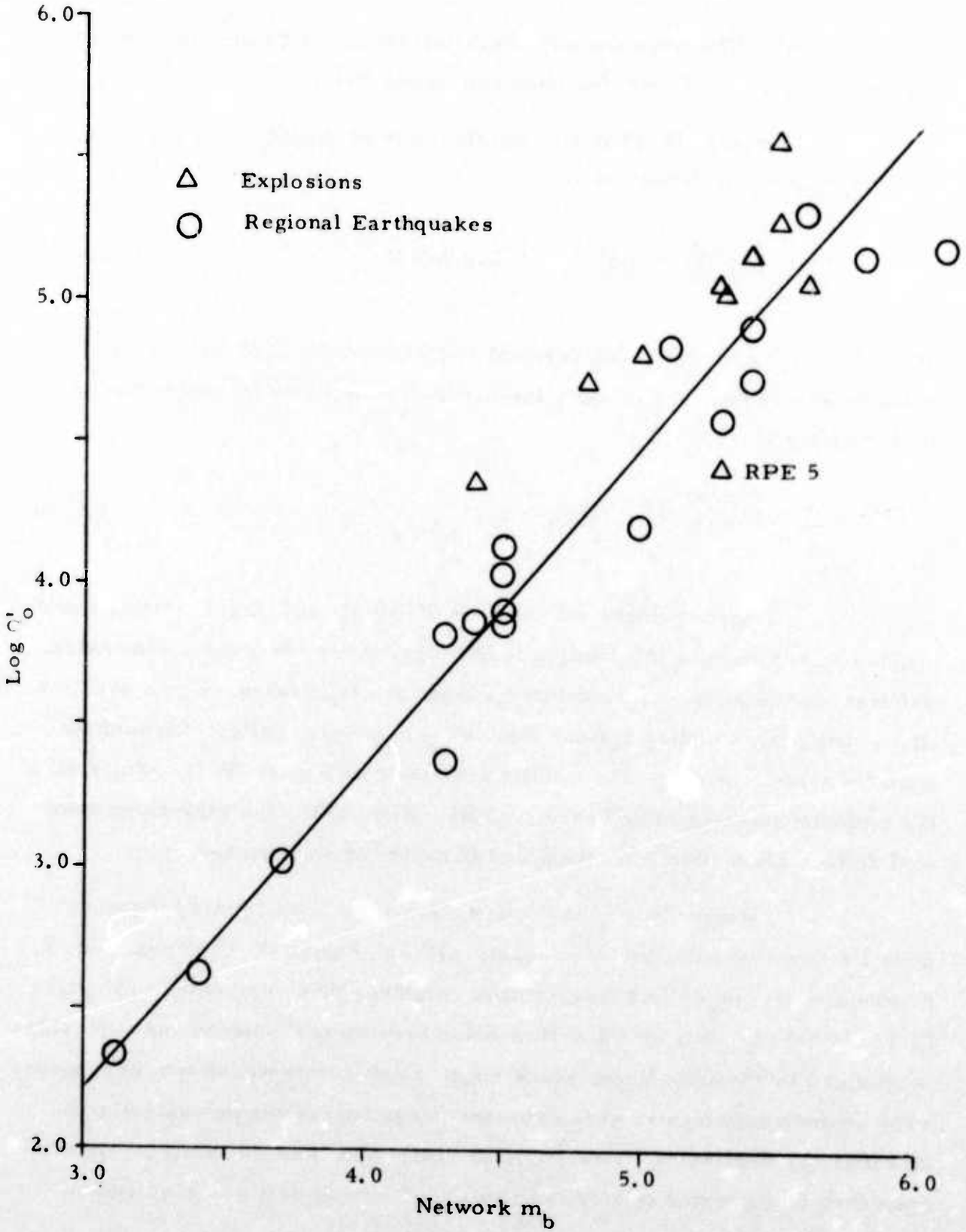

FIGURE IV-15

DISTANCE CORRECTED LOG OF THE DISPLACEMENT AMPLITUDE VERSUS NETWORK MAGNITUDE

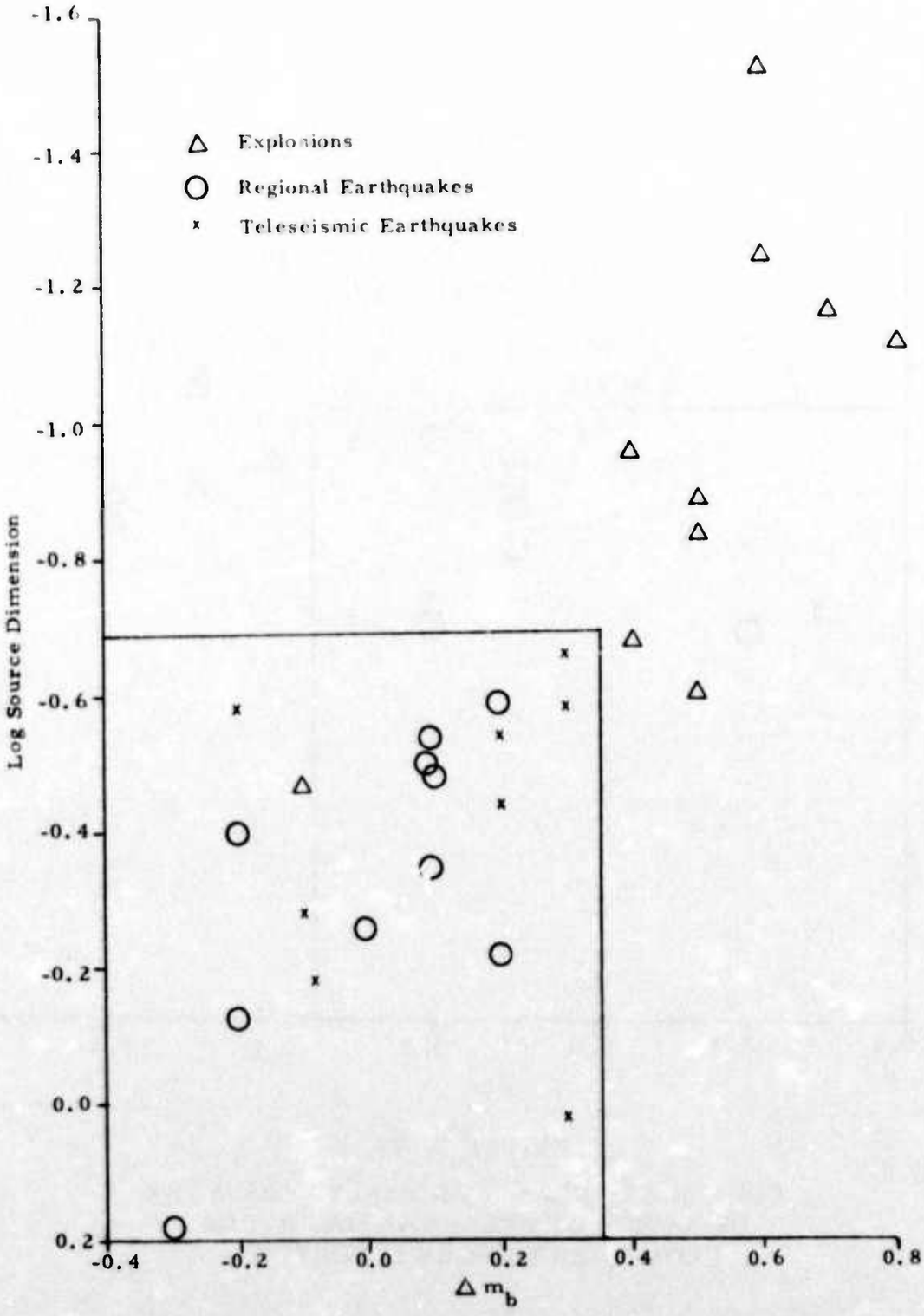

FIGURE IV-16

LOG SOURCE DIMENSION VERSUS THE DEVIATION OF SPECTRAL MAGNITUDE FROM NETWORK MAGNITUDE

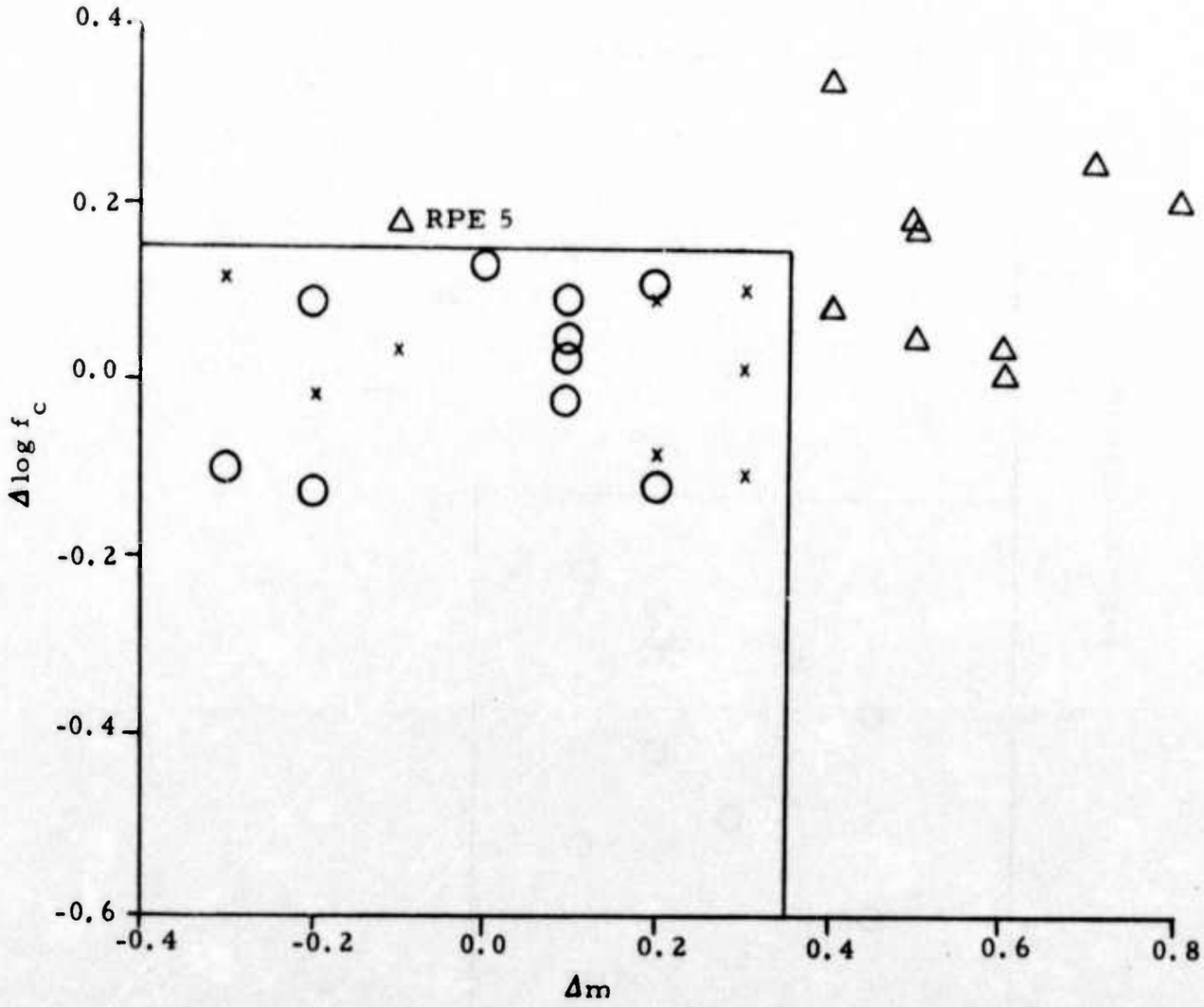

FIGURE IV-17

CORNER FREQUENCY ANOMALY VERSUS THE
DEVIATION OF SPECTRAL MAGNITUDE
FROM THE NETWORK MAGNITUDE

These results suggest that short-period spectral discriminants may provide at least supporting evidence for classification of events. More development of the maximum entropy spectrum, and a wider data base might well provide a discriminant powerful enough to be independent of other tests. We strongly recommend that such deve'opment be carried out.

Another important result of this work is the close correspondence between the spectral magnitudes found for regional events and the teleseismicly determined magnitudes (average of NOAA-PDE magnitudes) of these same events. This correspondence suggests that the spectral method may be a convienent and accurate means of determining the true magnitude of an event at regional distances. The absence of such a simple method for regional magnitude determination is the cause of a number of problems in seismology at present.

SECTION V
CONCLUSIONS AND RECOMMENDATIONS

The purpose of this study was to examine short-period spectral discriminants, and in particular discriminants based on corner frequency, which is expected to reflect differences in source dimensions. In order to do this a method of estimation based on the maximum entropy spectrum was developed. This method does away with the conventional assumption that the data are zero outside the sample interval, which is especially unrealistic for low signal-to-noise events. This result is achieved by estimating the autocorrelation function outside the data interval with a prediction error filter, and deriving the spectrum from this extended autocorrelation function. Tests on synthetic data showed that the shapes of spectra, and possibly the amplitudes as well, are quite satisfactory.

For high signal-to-noise ratio the spectra estimated in this way are in general agreement with those calculated by the conventional Fourier transform method, but show less ambiguity in their corner frequency. At low signal-to-noise ratio, Fourier methods cannot estimate these parameters at all, while the maximum entropy method yields clear-cut solutions in many cases.

In order to investigate the utility of the method as applied to the discrimination problem, P-wave maximum entropy spectra were watched for 28 earthquakes and presumed explosions.

To determine the internal consistency of the data, and to find if the data fit the model, corner frequencies calculated by energy considerations were compared with those measured directly from spectra. The agreement was quite satisfactory.

Corner frequencies measured directly from spectra were plotted against magnitude for the whole data sample. There was a general trend for events with larger magnitudes to have lower corner frequencies, but the scatter in the data was too great to effectively separate earthquakes and presumed explosions. Consequently we conclude that corner frequency by itself has very little discriminatory power.

A spectral magnitude, whose definition was motivated by that of spectral magnitudes calculated for local events, was found for the earthquake sample. It was a function of the zero-frequency spectral amplitude, the corner frequency, the epicentral distance, and one constant which was adjusted to minimize the variance between the spectral and network magnitudes. The network and spectral magnitudes found in this way were linearly related with a slope of nearly one. Then spectral magnitudes were found for the presumed explosions, using the relationship derived for earthquakes. These magnitudes were significantly higher than the corresponding network magnitudes, reflecting the higher radiated seismic energy associated with explosions. A discriminant based on this magnitude difference would have separated all earthquakes from explosions, and would have misclassified only one explosion.

The success of this single-valued discriminant lead to the search for a more powerful test using two parameters. A discriminant which appears to be effective combines the difference between spectral magnitude and conventional event magnitude with deviations of the corner frequency from the value obtained from a regression of corner frequency versus magnitude. This two dimensional plot of short-period discriminants indicated improved capability, but the data sample was still too small to draw reliable conclusions. The results suggest that a measure of source dimension has discriminating power and that further research on this topic is justified.

Some problems remain with maximum entropy spectra, however. In some situations additive random noise, coda, roundoff errors, and inherent limitations of the algorithm result in spectral power estimates less than zero at some frequencies. This is the most serious problem with the maximum entropy spectrum at this time.

In view of the improved spectra derived for events with low signal-to-noise ratio, and the more clear-cut measurements available from spectra with high signal-to-noise ratio as compared with conventional techniques, we recommend that more work on this subject be carried out. In particular, a more accurate maximum entropy spectral estimation technique should be developed. The improved method should be used to obtain accurate displacement spectrum of events for frequencies greater than 0.25 Hz. The method should be capable of minimizing errors due to ambient noise and coda. Given such an improved method, it should be applied to a broader data base comprising both teleseismic and regional events. The magnitude base lines of both types of events should be extended as far as possible to determine any magnitude limitations on the application of the discriminant.

SECTION VI
REFERENCES

Barnard, T. E., J. P. Burg, and G. D. Hair, 1969, Analytical studies of the techniques for the computation of high resolution wavenumber spectra, Advanced Array Research Special Report No. 9, Texas Instruments Incorporated, Dallas, Texas.

Brune, J. N., 1970, Tectonic stress and the spectra of seismic shear waves from earthquakes, J. Geophys. Res., 75, 4997-5009.

Hanks, T. C., and M. Wyss, 1972, The use of bodywave spectra in the determination of seismic source parameters, Bull. Seismol. Soc. Amer., 62, 561-590.

King, W. R., W. H. Swindell, and L. J. O'Brien, 1974, Final Report on a development of a curvilinear ray theory model and maximum entropy spectral analysis, Texas Instruments Incorporated, Dallas, Texas.

Peppin, W. A., 1967, The cause of bodywave surface wave discriminant between earthquakes and underground nuclear explosions at near-regional distances, Ph.D. Dissertation, University of California.

Richter, C. F., 1958, Elementary seismology, W. H. Freeman and Company, 366-367.

Seismic Data Laboratory Report No. 154, 1966, LRSM Measurements Pin Stripe, Alexandria, Virginia.

Thatcher, W., and T. C. Hanks, 1973, Source parameters of Southern California earthquakes, J. Geophys. Res., 78, 8547-8576.

Ulrych, T. J., D. E. Smylie, O. G. Jensen, and C. K. C. Clarke, 1973, Predicture filtering and smoothing of short records by using maximum entropy, J. Geophys. Res., 78, 23, 4959-4964.